Title: Rescuing lung development by embryonic inhibition of histone acetylation

Authors: Giangela Stokes[1], Zhuowei Li[1], Nicole Talaba[1], William Genthe[2], Maria E. Brix[2], Betty Pham[1], Mark D. Wienhold[3], Gracia Sandok[2], Rebecca Hernan[4], Julia Wynn[4], Haiyang Tang[5], Diana M. Tabima[6], Allison Rodgers[7], Timothy A. Hacker[7], Naomi C. Chesler[8], Pan Zhang[9], Rabi Murad[9], Jason Yuan[10], Yufeng Shen[11], Wendy K. Chung[12], David J. McCulley[1*]

Affiliations:

[1]Department of Pediatrics, University of California, San Diego, San Diego, CA 92093, USA.

[2]Department of Pediatrics, University of Wisconsin-Madison, Madison, WI 53705, USA.

[3]490 BioTech Inc., Knoxville, TN 37996, USA.

[4]Department of Pediatrics, Columbia University Irving Medical Center, New York, NY 10032, USA.

[5]State Key Laboratory of Respiratory Disease, National Clinical Research Center for Respiratory Disease, Guangzhou Institute of Respiratory Health, First Affiliated Hospital of Guangzhou Medical University, Guangzhou 510120, Guangdong, China.

[6]Department of Biomedical Engineering, University of Wisconsin-Madison, Madison, WI 53706, USA.

[7]Department of Medicine, University of Wisconsin-Madison, Madison, WI 53705, USA.

[8]Edwards Lifesciences Foundation Cardiovascular Innovation and Research Center and Department of Biomedical Engineering, University of California, Irvine, Irvine, CA 92697, USA.

[9]Sanford Burnham Prebys Medical Discovery Institute, La Jolla, CA 92037, USA.

[10]Section of Physiology, Division of Pulmonary, Critical Care and Sleep Medicine, Department of Medicine, University of California, San Diego, La Jolla, CA 92093, USA.

[11]Department of Systems Biology, Department of Biomedical Informatics, and JP Sulzberger Columbia Genome Center, Columbia University Irving Medical Center, New York, NY 10032, USA.

[12]Department of Pediatrics, Boston Children's Hospital, Harvard Medical School, Boston, MA 02115, USA.

***Corresponding author. Email:** dmcculley@health.ucsd.edu

One sentence summary: SIN3A is required for diaphragm and lung development in humans and mice by controlling the balance of histone acetylation.

Abstract: A major barrier to the impact of genomic diagnosis in patients with congenital malformations is the lack of clarity regarding how sequence variants contribute to disease pathogenesis and whether this information could be used to generate novel and patient-specific therapy. Congenital diaphragmatic hernia (CDH) is among the most common and severe of all structural malformations; however, its underlying mechanisms are unclear. We identified loss of function sequence variants in the epigenomic regulator gene *SIN3A* in two patients with complex CDH. Tissue-specific deletion of *Sin3a* in mice resulted in defects in diaphragm development, lung hypoplasia, and pulmonary hypertension, the cardinal features of CDH and major causes of CDH-associated mortality. Loss of SIN3A in the lung mesenchyme resulted in reduced cellular differentiation, impaired cell proliferation, and increased DNA damage. Treatment of embryonic *Sin3a* mutant mice with anacardic acid, an inhibitor of histone acetyltransferase, increased differentiation and cell proliferation while reducing DNA damage. These findings demonstrate that restoring the balance of histone acetylation is an effective strategy to improve lung development in the *Sin3a* mouse model of CDH.

Main text:

INTRODUCTION

Congenital malformations remain the leading cause of infant mortality in the United States and are a significant source of newborn morbidity (*1*). One of the most common and severe anomalies is congenital diaphragmatic hernia (CDH) which occurs in 1 out of every 3000-3500 live births with a mortality rate of 10-50% (*2-8*). Although abnormal diaphragm development is the hallmark of the disease, the high rate of morbidity and mortality in patients with CDH is due to defects in lung and pulmonary vascular development causing lung hypoplasia and pulmonary hypertension (*9, 10*). Despite the frequency and severity of CDH, the underlying developmental mechanisms are not well understood. Genetic studies in patients and families have identified a growing list of CDH candidate genes implicated in development of the diaphragm (*11-15*). Loss of function studies of these genes in animal models have demonstrated impaired diaphragm development as well as a direct role for genetic mutations in the mechanisms responsible for lung hypoplasia and pulmonary hypertension (*16-21*).

Epigenetic regulation of gene expression plays an important role throughout development and in physiological adaptation to birth (*22-26*). Defects in epigenetic regulation of gene expression have been implicated in the mechanisms responsible for human disease including neurodevelopmental disorders and structural malformations such as congenital heart disease and neural tube defects (*24, 27-36*). Global disruption of DNA methylation or histone deacetylation, two of the most well studied epigenetic mechanisms of gene regulation, results in early embryonic lethality (*37-40*). In the lungs, regulation of histone acetylation has been shown to be important for development and in the mechanisms responsible for asthma, chronic obstructive pulmonary disease, pulmonary fibrosis, lung cancer, and pulmonary hypertension (*41-52*). The

balance of gene transcription and repression maintained by histone acetylation is controlled by the complementary activity of histone acetyltransferase (HAT) and histone deacetylation (HDAC) enzymes (*52-54*). The tightly coordinated activity of these enzymes is necessary for rapid changes in gene expression that occur during embryonic development and in disease (*55-58*).

To direct the timing, cell, and genome region-specific action of histone deacetylases, HDAC1 and HDAC2 form multi-protein complexes (*59-62*). The SIN3-HDAC complex is one of several such complexes that regulate histone deacetylation (*63-68*). The SIN3/HDAC complex is most well-known for its role in transcriptional repression by histone deacetylation and regulation of cell cycling during development (*64-71*). Because SIN3A can also activate transcription, it has become recognized as a transcriptional co-regulator whose function depends on interactions with a wide range of DNA-binding co-factors (*70, 72-79*). During development, SIN3A plays multiple roles in both organogenesis and cell lineage specification while loss of SIN3A has been reported to cause defects in energy metabolism and impaired cell cycling (*80-87*). Relevant to CDH, SIN3A was demonstrated to play a role in skeletal muscle cell development, maintenance, and function (*88*). In the developing lungs, loss of SIN3A in foregut endoderm derived epithelium resulted in failure of branching morphogenesis and cell cycle arrest (*89*). In adult mice, conditional deletion of *Sin3a* in type 2 alveolar epithelial cells resulted in p53-dependent senescence and pulmonary fibrosis (*90*). Haploinsufficiency or sequence variants in the *SIN3A* gene have been reported in human patients with Witteveen-Kolk syndrome (OMIM 613406) and characteristic neurocognitive impairment, growth and feeding difficulties, and distinctive facial features (*91-96*). Interestingly, despite the importance of SIN3A in regulating

development, to our knowledge, there are no prior reports of *SIN3A* sequence variants in patients with congenital malformations.

To understand the genetic and developmental mechanisms responsible for CDH, we conducted whole genome sequencing in patients and family members with the disease. Small deletions that resulted in heterozygous loss-of-function of *SIN3A* were identified in two patients with complex CDH. To determine the role that SIN3A plays in development of the diaphragm and lung mesenchyme, we conducted tissue specific deletion of *Sin3a* in mice. We found that SIN3A is required in the skeletal muscle and mesothelium for diaphragm formation. Furthermore, in the lung mesenchyme, SIN3A is required for cellular differentiation, cell cycling, and regulation of DNA damage. Although SIN3A controls gene expression through multiple mechanisms, we found that loss of SIN3A resulted in an imbalance of histone acetylation and deacetylation which was restored by embryonic inhibition of histone acetyltransferase.

RESULTS

SIN3A loss-of-function sequence variants were identified in patients with CDH

To identify genetic mechanisms responsible for CDH, whole genome or exome sequencing was conducted on 827 patient and parent trios enrolled in the Diaphragmatic Hernia Research and Exploration; Advancing Molecular Science (DHREAMS) study (*15, 97*). Among the 1,153 protein-coding variants identified in this cohort were 418 gene damaging variants discovered in 318 of the CDH patients (38.4%) (*15*) including *de novo*, two and seven base pair frameshift deletions in the *SIN3A* gene in two patients with complex CDH (Figure 1A, B). One of these patients, who had a two base pair deletion and frameshift variant in exon 18, died during the newborn period with a severe, multi-system, phenotype including right-CDH, respiratory failure, coarctation of the aorta, imperforate anus, and limb abnormalities (Figure 1B, Supplemental Table 1). The second patient, who had a seven base pair deletion and frame shift variant in exon 11, also had a multi-system phenotype with left-CDH, unilateral pelvic kidney, and a palate defect but less severe lung and pulmonary vascular disease and developed schizoaffective disorder (Figure 1B, Supplemental Table 1). Although growth and neurodevelopmental disorders have been described in patients with *SIN3A* gene variants and Witteveen-Kolk syndrome (*93, 96*), to our knowledge, this is first report of congenital diaphragmatic hernia identified in patients with damaging *SIN3A* sequence variants.

To determine if disruption of SIN3A function might lead to CDH phenotypes including diaphragm malformation, pulmonary hypertension, or lung hypoplasia, expression of *Sin3a* was characterized in mice. *Sin3a* expression was identified in both the developing diaphragm and throughout the lungs at embryonic day 12 (E12, Figure 1C-E). In addition to its reported expression in the endoderm derived epithelium (Figure 1G) (*89*), *Sin3a* is expressed throughout

the developing lung mesenchyme during embryonic and early postnatal stages (Figure 1F-H, Supplemental Figure 1A-E) including in *Pdgfrα*-expressing myofibroblast, *Plin2*-expressing lipofibroblast, *Sm22α*-expressing airway and vascular smooth muscle cells, and *Erg*-expressing lung endothelial cells (Supplemental Figure 1F-H).

SIN3A is required in the skeletal muscle and mesothelium for diaphragm development

To determine if SIN3A is required for diaphragm formation, conditional deletion of *Sin3a* was conducted using cell-specific Cre-recombination in cell populations that compose the diaphragm. To investigate the role of SIN3A in the developing diaphragm fibroblasts, *Prx1-Cre* was used to induce recombination in lateral plate mesoderm-derived fibroblast cells that express *Sin3a* (Figure 2A, B). Compared to controls (Figure 2C, Supplemental Figure 2A-E), *Prx1-Cre; Sin3a* conditional deletion embryos (CKO) exhibited abnormal limb formation (Supplemental Figure 2F), but normal diaphragm development with *Tcf4*-expressing fibroblast cells, *Myod1*-expressing skeletal muscle cells, and *Wt1*-expressing mesothelial cells (Figure 2D and Supplemental Figure 2G-J).

To determine if SIN3A is required in the skeletal muscle during diaphragm development, *Pax3-Cre* was used to induce recombination in somatic mesoderm-derived skeletal muscle that expresses *Sin3a* (Figure 2E, F). Compared to controls (Figure 2G and Supplemental Figure 2A-E), *Pax3-Cre; Sin3a* CKO embryos had a thin, membranous, and muscle-less diaphragm (Figure 2H and Supplemental Figure 2L), in addition to other structural defects including anencephaly (Supplemental Figure 2K). The diaphragm of *Pax3-Cre; Sin3a* CKO embryos did not contain *Tcf4*-expressing fibroblast or *Myod1*-expressing skeletal muscle cells and was composed exclusively of *Wt1*-expressing mesothelial cells (Supplemental Figure 2M-O).

To determine if SIN3A is required in diaphragm mesothelial cells, *Tbx4-rtTA; Tet-o-Cre* was used to induce recombination in the developing mesothelium that expresses *Sin3a* beginning at embryonic day 6 (Figure 2I, J). Compared to controls (Figure 2K and Supplemental Figure 2A-E), deletion of *Sin3a* using this approach resulted in a left, posterior-lateral defect of the diaphragm with herniation of the stomach, intestine, and liver into the left-thorax (Figure 2L and Supplemental Figure 2P, Q). This left posterior-lateral diaphragm defect is seen in the majority of patients with CDH. The remaining diaphragm of *Tbx4-rtTA; Tet-o-Cre; Sin3a* CKO embryos contained *Tcf4*-expressing fibroblast, *Myod1*-expressing skeletal muscle, and *Wt1*-expressing mesothelial cells (Supplemental Figure 2R-T). At the site where the diaphragm failed to close there was decreased expression of *Tcf4*, normal expression of *Myod1*, and increased and disorganized expression of *Wt1* within the pleuroperitoneal fold (PPF, Supplemental Figure 2U-W). Taken together, these data suggest that SIN3A is required in both the somatic mesoderm derived skeletal muscle and the mesothelium during diaphragm development.

SIN3A is required in the lung mesenchyme

To investigate the role of SIN3A during lung development, *Tbx4-rtTA; Tet-o-Cre* was used to induce deletion of *Sin3a* beginning at embryonic day 6 (Supplemental Figure 3A), resulting in recombination throughout the lung mesenchyme as well as in the diaphragm (Supplemental Figure 3B). *Tbx4-rtTA; Tet-o-Cre; Sin3a* CKO mice were born at the expected Mendelian ratio, but all died after birth (Supplemental Figure 3C). Compared to controls (Supplemental Figure 3D), deletion of *Sin3a* using this approach resulted in left-CDH with liver herniation into the thorax (Supplemental Figure 3E). Gross inspection of the trachea and lungs demonstrated that *Tbx4-rtTA; Tet-o-Cre; Sin3a* CKO mice had lung hypoplasia (Supplemental

Figure 3F). Histological analysis of the embryonic thorax revealed that *Tbx4-rtTA; Tet-o-Cre; Sin3a* CKO mice had left-CDH, rightward deviation of the heart, liver herniation, and lung hypoplasia (Supplemental Figure 3H). To determine if lung hypoplasia in *Tbx4-rtTA; Tet-o-Cre; Sin3a* CKO mice occurred independent of mechanical compression by herniated abdominal organs, mutant lungs were compared to controls at E12, prior to organ herniation (Supplemental Figure 3I). Despite the loss of SIN3A, E12 *Tbx4-rtTA; Tet-o-Cre; Sin3a* CKO lungs were similar to controls (Supplemental Figure 3I).

To investigate the role of SIN3A during later stages of lung mesenchymal development without mechanical compression caused by herniated abdominal organs, doxycycline was used to induce recombination throughout the lung mesenchyme beginning at embryonic day 12 (Figure 3A, B). Using this approach, compared to controls that had *Sin3a* expression throughout the lungs (Figure 3C), *Tbx4-rtTA; Tet-o-Cre; Sin3a* CKO mice (referred to hereafter as *Sin3a* CKO) lacked expression of *Sin3a* in the mesenchyme but retained its expression in the epithelium (Figure 3D). Despite appearing normal at birth and surviving into adulthood, *Sin3a* CKO mice did not gain weight as rapidly as controls (Figure 3E, F). Histological analysis at P28 revealed that *Sin3a* CKO mice had emphysematous dilation of the distal airspaces (Figure 3H). Like newborn patients with CDH, *Sin3a* CKO mice had defects in pulmonary vascular development (Figure 3I-L) including decreased lung vessel number and increased vascular smooth muscle wall thickness (Figure 3K, L) as well as pulmonary hypertension with right ventricular hypertrophy, increased pulmonary vascular resistance, decreased right ventricular function, and increased right peak systolic pressure (Figure 3M-P). Despite having normal lung size at birth (Figure 3Q), the first histological evidence of abnormal lung structure was present in *Sin3a* CKO mice at P0 with thickened interstitium and simplified air spaces (Figure 3R-T).

Pulmonary vascular defects were also present at P0 in *Sin3a* CKO mice with decreased lung vessel number but not vascular smooth muscle hypertrophy (Figure 3U-X).

SIN3A is required in the lung mesenchyme for myofibroblast, extracellular matrix, endothelial, and alveolar epithelial cell development

To determine the impact of SIN3A loss of function during lung mesenchymal development, the number and type of lung mesenchymal cells were analyzed in control and *Sin3a* CKO lungs. Compared to controls (Figure 4A), *Sin3a* CKO lungs had fewer mesenchymal cells (Figure 4B, C). Loss of SIN3A resulted in decreased *Pdgfra*-GFP-labelled myofibroblast precursor cells, extracellular matrix, and *Elastin* gene expression compared to controls (Figure 4D-I). In contrast, lipofibroblast cells were not clearly impacted by the loss of SIN3A (Figure 4J-L). These data demonstrate that SIN3A plays a primary role in lung mesenchymal cell development in addition to its role in diaphragm formation.

Supporting the idea that the mesenchyme plays a central role in directing embryonic lung development, mesenchyme-specific deletion of *Sin3a* resulted in decreased ERG-labelled alveolar endothelial cells, SPC-labelled type-2 alveolar epithelial cells, and HOPEX-labelled type-1 alveolar epithelial cells compared to controls (Figure 4 M-U).

To investigate the role of SIN3A in vascular development during lung formation, *Cdh5-Cre* was used to delete *Sin3a* in developing endothelial cells (Supplemental Figure 4A). *Cdh5-Cre Sin3a* CKO embryos initiate lung development and appear healthy at E11 (Supplemental Figure 4B-E) but develop diffuse hemorrhage between E11-12 and fail to undergo branching morphogenesis (Supplemental Figure 4B, F-H). These data demonstrate the essential role that SIN3A plays in endothelial cells for embryonic vascular development.

SIN3A is required for regulation of cell cycling and DNA damage

SIN3A has been demonstrated to direct multiple mechanisms necessary for development including regulation of cell cycling and cellular differentiation. To determine if SIN3A plays a similar role in the developing lung mesenchyme, cell proliferation, cell death, and DNA damage were investigated in *Sin3a* CKO mice. Compared to controls (Figure 5A, D), *Sin3a* CKO lungs had a similar number of phosphohistone H3 (PPH3)-positive dividing cells (Figure 5B, C), but fewer EDU-positive cells undergoing G1 to S-phase transition (Figure 5E, F). Additionally, compared to controls (Figure 5G), *Sin3a* CKO mice had more cleaved caspase 3 (CC3)-positive cells undergoing apoptosis (Figure 5H, I). Finally, because loss of SIN3A has been shown to result in increased DNA damage (*98*), H2AX staining was used to quantify the number of cells with evidence of DNA damage. Compared to controls (Figure 5J), *Sin3a* CKO lungs had an increase in the number of H2AX stained cells (Figure 5K, L). These data suggest that loss of SIN3A function in the lung mesenchyme resulted in decreased G1 to S-phase transition, increased programmed cell death, and increased DNA damage.

Loss of SIN3A transcriptional regulation resulted in impaired lung mesenchymal cell differentiation

To identify the genetic mechanisms responsible for abnormal lung development due to the loss of SIN3A, RNA was collected from the lungs of four control and four *Sin3a* CKO mice at 3 stages (Supplemental Figure 5A) including E16, when defects in cell cycling and DNA damage were first evident (Figure 5D-F and J-L) and when expression of *Sin3a* was highest (Supplemental Figure 1A), P0 when the histological phenotype was first evident (Figure 3L-N)

and when there were changes in the number of mesenchymal, endothelial, and alveolar epithelial cells (Figure 4A-F and M-U), and P3 when there was a reduction in the extracellular matrix (Figure 4G-I). Expression of more than 200 genes was altered in *Sin3a* CKO mice at each stage (Supplemental Tables 3-5) and 37 genes were mis-regulated by the loss of SIN3A at all stages (Supplemental Figure 5A). Consistent with the known role of SIN3A as a transcriptional repressor, deletion of *Sin3a* resulted in increased expression of most of these genes (Supplemental Figure 5B). Among these 37 genes were those expressed in proliferative lung mesenchymal progenitor cells and that encode regulators of cell cycle progression or G1 to S-phase transition including *Rnf26*, *Cyp46a1*, *Ccne1*, *Hectd3*, *Rrp12*, *Wdr55*, and *Tmem231* (Supplemental Figure 5A, B).

To investigate the changes in gene expression that occurred specifically in lung mesenchymal cells, flow cytometry was used to isolate mesenchymal cells that underwent recombination indicated by the presence of a CRE-responsive red-fluorescence reporter protein from four control and four *Sin3a* CKO mice at E16. Compared to controls, *Sin3a* CKO lung mesenchymal cells had differential expression of more than 4000 genes (Figure 6A). In contrast to the whole lung gene expression analysis (Supplemental Figure 5A, B), the number of genes with increased expression (2155) was similar to the number with decreased expression (2010) in recombined *Sin3a* CKO mesenchymal cells (Figure 6A). Among the 100 most significantly mis-regulated genes were 9 identified in the shared whole-lung gene-expression experiment (*Gba*, *Ift22*, *Qdpr*, *Rpp40*, *Cyp46a1*, *Evi5l*, *Rcl1*, *Wdr55*, and *Klf16*) as well as genes expressed in myofibroblasts (*Des*), lipofibroblasts (*Baz1a*), and extracellular matrix (*Gsto1*, *Adamts4*, *Crtac1*, *Col9a2*, *Scara3*, and *Col16a1*, Figure 6A). Also among the 100 most significantly mis-regulated genes were those encoding members of the apoptosis pathway (*Sod2*, *Ing2*, *Aen*, and *Mnt*),

involved in DNA repair (*Cep164*, *Cenpx*, *Sirt7*, and *Chaf1b*), and SIN3 associated proteins (SAPs: *Ing2*, *Ing1*, and *Sap30*, Figure 6A).

Because impaired mesenchymal cell development was a predominant phenotype observed in the *Sin3a* CKO lungs, we compared the differentially expressed genes to a recently published reference list of genes expressed in mesenchymal cell sub-populations and their precursors (*99*). Compared to controls, *Sin3a* CKO mesenchymal cells had decreased expression of myofibroblast, matrix fibroblast, and lipofibroblast genes (Figure 6B). In contrast, expression of proliferative progenitor genes was increased in *Sin3a* CKO mesenchymal cells (Figure 6B). These data were confirmed by qRT-PCR conducted using RNA from whole lungs of E16 *Sin3a* CKO and littermate control mice (Figure 6B) and suggest that loss of SIN3A resulted in impaired lung mesenchymal cell differentiation.

To investigate the impact of *Sin3a* deletion on mesenchymal cell differentiation, recombined lung mesenchymal cells collected from two control and two *Sin3a* CKO embryos were analyzed using single-cell RNA sequencing at E16 (Supplemental Figure 6). Using this approach, recombined mesenchymal cells were organized into 14 clusters and broadly categorized as proliferative mesenchymal progenitor cells (PMPs), undifferentiated transitional mesenchymal cells, or differentiating mesenchymal precursor cells (Figure 6C, Supplemental Figure 7). Comparison of the lung mesenchymal cells collected from the two control and the two *Sin3a* CKO mice (Figure 6D) demonstrated an increase in the relative number of proliferative progenitor cells and a decrease in differentiating myofibroblast, matrix, and *Ebf1*-expressing lung fibroblast precursor cells from *Sin3a* CKO mice (Figure 6E, Supplemental Figure 8, Supplemental Table 6). The reduction in differentiating mesenchymal precursor cells was most significant in the myofibroblast cells (Figure 6E, Supplemental Table 6). These results are similar

to the histological data (Figure 4D-I) and sorted lung mesenchymal gene expression analysis (Figure 6B) and suggest that defects in lung development in *Sin3a* CKO mice were due to failure of cell differentiation.

SIN3A is required for lung myofibroblast and matrix fibroblast differentiation

Analysis of spliced and un-spliced transcripts using RNA velocity demonstrated the pattern of differentiation from proliferative mesenchymal cells to transitional undifferentiated mesenchymal cells and then to differentiating mesenchymal precursor cells in control and *Sin3a* CKO lung mesenchymal cells (Figure 6F). To determine how *Sin3a* deletion affected the potential for cell differentiation, we analyzed the RNA velocity lengths (*100*) which were reduced in mesenchymal cells collected from *Sin3a* CKO mice compared to controls (Figure 6G, H). The decrease in RNA velocity lengths was observed in PMP, transitional undifferentiated mesenchymal cells, and in differentiating mesenchymal precursor cells (Figure 6H). These data suggest that loss of SIN3A resulted in decreased differentiation potential of mesenchymal cells at all stages of differentiation.

To determine the genetic mechanisms responsible for reduced mesenchymal cell differentiation, integrated pathway analysis (IPA) was used to identify pathways mis-regulated by the loss of SIN3A (Figure 7A). The most significantly mis-regulated canonical and process pathways were pathways relevant for lung development and the phenotype observed in *Sin3a* CKO lungs including idiopathic pulmonary fibrosis, lung formation, vascular development, entry into S-phase, fibroblast cell death, and senescence where SIN3A has been shown to play a role in lung epithelial cells (Figure 7A) (*90*). The mis-regulated upstream regulator pathways included several that play an important role in mesenchyme and lung myofibroblast development and

differentiation specifically (Figure 7A-C) including decreased expression of myofibroblast and matrix fibroblast genes (*Acta2*, *Myh11*, *Tagln*, *Tgfbi*, *Des*, *Igfbp5*, *Eln*, *Igfbp4*, *Jund*, and *Mmp2*, Figure 7B) and decreased expression of TGFB and WNT pathway genes (*Fos*, *Jun*, *Col1a1*, *Col3a1*, *Col4a1*, *Col6a3*, and *Fzd2*, Figure 7C). These findings were confirmed using the RNA-sequencing analysis conducted on sorted lung mesenchymal cells (Figure 6A) and gene expression analysis conducted on whole lung RNA extracts at E16 which demonstrated a similar reduction in TGFB and WNT gene expression in *Sin3a* CKO lungs (Figure 7C). Together these data suggest that loss of SIN3A resulted in altered gene expression in pathways required for myofibroblast and matrix fibroblast differentiation.

SIN3A deletion altered gene expression that impaired cell cycling, DNA damage, and senescence

In addition to the changes in mesenchymal cell differentiation, pathway and differential gene expression analysis of *Sin3a* CKO mesenchymal cells demonstrated decreased entry into S-phase (Figure 7A) with decreased expression of genes that promote cell cycle progression (*H19*, *Id3*, *Ccnd2*), increased expression of genes associated with cell cycle arrest, cell death, or senescence (*Ccne1*, *Bax*, *Sod2*, *Ing1*), and increased expression of *Ing2*, one of the SIN3 associated proteins (SAPs, Figure 7D). These findings were confirmed using the sorted lung mesenchymal RNA-sequencing analysis (Figure 6A) and gene expression analysis conducted on RNA extracted from E16 control and *Sin3a* CKO lungs (Figure 7E-H). Loss of SIN3A resulted in reduced expression of genes that promote mesenchymal cell proliferation and increased expression of genes that promote cell cycle arrest (Figure 7E). *Sin3a* CKO mice also had increased expression of genes expressed in response to DNA damage and altered expression of

genes associated with DNA repair (Figure 7F). These data support the conclusion that SIN3A is required during lung development to promote mesenchymal cell differentiation and that loss of SIN3A resulted in impaired cell cycling and increased DNA damage.

Pathway and single cell gene expression analysis demonstrated that loss of SIN3A resulted in increased expression of genes involved in senescence (Supplemental Figure 9A, G). SIN3A has been demonstrated to regulate genes implicated in senescence and loss of SIN3A in the lung epithelium was associated with senescence and pulmonary fibrosis (*89, 90*). Compared to controls, *Sin3a* CKO mesenchymal cells had differential expression of multiple genes associated with senescence (Supplemental Figure 9G). This expression analysis did not indicate an increase or decrease in senescence activation as genes that promote or repress senescence were both positively and negatively impacted by the loss of SIN3A (Supplemental Figure 9G). These data suggest that loss of SIN3A in the mesenchyme resulted in an accumulation of progenitor cells, decreased cell cycling, increased DNA damage, and senescence.

SIN3A is required for controlling the balance of histone acetylation

SIN3A regulates gene expression through multiple mechanisms including histone and DNA methylation and demethylation (add ref). Gene expression analysis of sorted lung mesenchymal cells from *Sin3a* CKO and control lungs at E16 demonstrated increased expression of genes that promote both histone methylation and demethylation whereas genes that promote DNA methylation or demethylation were decreased (Figure 7G). Gene expression conducted on whole lung RNA extracts from *Sin3a* CKO and control mice at E16 did not demonstrate a consistent trend in either histone or DNA methylation (Figure 7G). Because more of the genes that direct histone methylation or demethylation were mis-regulated in *Sin3a* CKO recombined

mesenchymal cells, immunofluorescence staining for transcriptional repressing methylation of histone 3 lysine 9 (H3K9Me2 and H3K9Me3) and lysine 27 (H3K27Me3) was conducted at E16 (Supplemental Figure 10A-I). These data demonstrate that no significant change in histone methylation was detectable despite the loss of SIN3A during lung mesenchymal development (Supplemental Figure 10A-I).

SIN3A is known to act as a transcriptional repressor through its cooperative interaction with HDACs. The activity of the SIN3/HDAC complex is modulated by multiple co-factors (*63, 79, 101*). In recombined *Sin3a* CKO lung mesenchymal cells at E16 (Figure 6A), expression of the SIN3-HDAC core complex and SIN3 associated protein (SAP) genes was up-regulated including *Sap30*, *Sap18*, *Suds3*, *Arid4b*, *Rb1*, *Brms1*, *Sap130*, *Sap25*, *Ing1*, *Ing2*, *Sin3b*, and *Mxi1* (Figure 7H). These data were confirmed by gene expression analysis conducted on whole lung RNA extracts from *Sin3a* CKO and control embryos at E16 demonstrating mis-regulated expression of both core SIN3/HDAC and SAP co-factors (Figure 7H). In contrast, expression of histone acetyltransferase genes *Crebbp* and *Ep300* was not changed in lung mesenchymal cells from *Sin3a* CKO embryos (Supplemental Figure 11 A, B).

To determine if loss of SIN3A in the lung mesenchyme had a direct impact on the balance of histone acetylation, immunofluorescence staining for transcriptional activating acetylation of H3K9 and H3K27 was conducted on *Sin3a* CKO and control lungs (Figure 8A-F). These data demonstrate that loss of SIN3A resulted in increased histone acetylation in *Sin3a* CKO lungs (Figure 8C, F, G). The imbalance of histone acetylation and deacetylation observed in *Sin3a* CKO lungs might be responsible for the observed changes in gene expression as well as the decrease in mesenchymal cell differentiation, decrease in cell cycling, and increase in DNA damage.

To investigate this hypothesis and determine if embryonic inhibition of histone deacetylation recapitulates SIN3A loss of function, control and *Sin3a* CKO mice were treated with the HDAC-inhibitor trichostatin A (TSA) beginning when doxycycline induced recombination was initiated (Figure 8N) (*102, 103*). Using this approach there was no difference in the number of EDU-positive cells in untreated *Sin3a* CKO lungs (Figure 8I) compared to those treated with DMSO vehicle control (Supplemental Figure 12B, C) or those treated with TSA (Supplemental Figure 12H, I). In contrast, compared to untreated control lungs (Figure 8H) or those treated with DMSO (Supplemental Figure 12A) there was a reduction in the number of EDU-positive cells in control lungs treated with TSA (Supplemental Figure 12G, I). The number of EDU-positive cells in control lungs treated with TSA was similar to the number of EDU-positive cells in untreated *Sin3a* CKO lungs (Figure 8I, Supplemental Figure 12G, I). These data suggest that embryonic HDAC-inhibition with TSA resulted in decreased G1 to S-phase transition that was similar to loss of SIN3A function. Interestingly, HDAC-inhibition with TSA did not alter the number of cells with evidence of DNA damage indicated by H2AX staining in either *Sin3a* CKO or control lungs (Figure 8K-M compared to Supplemental Figure 12D-F and J-L) suggesting that DNA damage observed in *Sin3a* CKO mice might not be due to decreased HDAC function alone.

SIN3A loss-of-function can be restored by inhibition of histone acetyltransferase

To determine if the balance of histone acetylation and deacetylation could be restored despite the absence of SIN3A, we treated embryos with A-485, a potent inhibitor of HAT p300/CPB (*104*). *Sin3a* CKO lungs treated with A-485 demonstrated decreased DNA damage (Supplemental Figure 12Q, R) compared to untreated mutant lungs (Figure 8L). Interestingly,

although DNA damage was reduced in the mutant lungs with A-485, G1 to S-phase transition remained decreased in *Sin3a* CKO lungs (Supplemental Figure 12N, O compared to Figure 8I). G1 to S-phase transition was also decreased in control lungs treated with A-485 (Supplemental Figure 12M, O) compared to those that were untreated (Figure 8H). These data suggest that potent inhibition of p300/CBP HAT by A485 can make DNA resistant to damage but not accessible for replication during lung development. These findings support the idea that SIN3A plays an important role in regulating the balance of histone acetylation and deacetylation.

To investigate this hypothesis further, anacardic acid (AA), a naturally occurring HAT inhibitor that is 1000 times less potent than A-485 (*102, 104, 105*), was used to treat *Sin3a* CKO and control mice following the regimen conducted with TSA and A-485 (Figure 8N). Our rationale for using a less potent HAT inhibitor was that partial inhibition of acetyltransferase might restore the balance of histone acetylation while maintaining sufficient histone acetylation necessary for DNA replication and cell proliferation. Using this approach, no difference was observed in histone acetylation in untreated control embryos (Figure 8A, D) or those treated with AA (Figure 8O, Q, R, T) whereas histone acetylation was decreased in AA treated *Sin3a* CKO embryos (Figure 8P, Q, S, T) compared to untreated *Sin3a* CKO embryos (Figure 8B, E). Using the same embryonic treatment, no difference was observed in the number of EDU-positive cells or in the number of cells with evidence of DNA damage in control lungs treated with AA (Figure 8 U, W, X, Z) compared to those that were untreated (Figure 8H, K). In contrast, the number of EDU-positive cells was increased while the number of cells with evidence of DNA damage was decreased in *Sin3a* CKO lungs treated with AA (Figure 8 V, W, Y, Z) compared to those that were untreated (Figure 8I, L).

To determine if the increased cell proliferation and decreased DNA damage observed in *Sin3a* CKO embryos following AA treatment were due to inhibition of p300-CBP specifically, we treated with diluted A485 to mimic the potency of AA HAT inhibition. A485 was developed to be a specific inhibitor of p300/CBP (PMID: 28953875). We found that both 1:100 and 1:1000 dilutions of A485 were sufficient to increase cell proliferation and decrease DNA damage in *Sin3a* CKO embryos (Supplemental Figure 12S-D' compared to Figure 8H-M). These data suggest that partial inhibition of histone acetyltransferase with either AA or A485 was sufficient to restore the balance of histone acetylation despite the loss of SIN3A. This conclusion was further supported by the finding that AA treatment resulted in an increased number of *Pdgfra*-GFP positive myofibroblast precursor cells in *Sin3a* CKO lungs compared to untreated controls and *Sin3a* CKO lungs that were untreated (Figure 8A'-E'), reduced apoptosis to the level observed in controls (Supplemental Figure 13A-F), improved saccular development of the *Sin3a* CKO lungs (Figure 8F'-J'), and increased lung vessel number (Figure 8K'-O'). In addition to these observed improvements in development, pulmonary vascular physiological function was also improved in *Sin3a* CKO mice following treatment with AA. Compared to vehicle control treated mice, *Sin3a* CKO mice treated with AA had reduced right ventricular hypertrophy (Fulton's index, Figure 8Q') and reduced pulmonary vascular resistance (RVSP, Figure 8R').

These data support the idea that epigenetic regulation of gene expression is controlled by a balance of histone acetylation and deacetylation during embryonic development (Figure 9). Loss of this balance either by genetic deletion of a critical co-factor, like SIN3A, or by pharmacological inhibition of histone acetyltransferase or HDAC results in impaired cell cycling, DNA damage, and impaired cellular differentiation. Partial inhibition of histone acetyltransferase is sufficient to restore this balance in lung mesenchymal cells that lack SIN3A.

DISCUSSION

Regulation of histone acetylation is required to direct the rapid changes in gene expression and DNA replication necessary during development (*106-112*). The complementary activity of histone acetyltransferase (HAT) and histone deacetylase (HDAC) enzymes maintains the balance of histone acetylation and therefore controls transcriptional activation or repression as well as DNA replication (*108, 112-114*). The balance of HAT and HDAC activity itself is necessary for development (*57, 115, 116*); however, how failure to maintain this balance contributes to congenital malformations is not clear. Here we focused on an essential component of the HDAC co-regulatory complex, SIN3A, and showed that loss of SIN3A function in the developing diaphragm and lungs caused failure of diaphragm formation and lung defects similar to those observed in patients with CDH. In the developing lungs, SIN3A was required to maintain the balance of histone acetylation whereas loss of SIN3A resulted in defects in lung development and pulmonary hypertension, the two major contributors to mortality in patients with CDH.

The SIN3/HDAC complex is one of many chromatin modifiers that regulate gene expression and DNA replication by controlling the open or compact state of chromatin and thus access of transcription or replication factors to DNA (*63, 117, 118*). During development, chromatin modifications themselves are affected by changes in the environment, including exposures to toxins and changes in the mother's health, and translate these changes to the developing embryo (*117*). These interactions are especially important in human structural malformations where there is an overlapping impact of pathogenic gene variants and environmental mechanisms that contribute to the underlying defects in development (*119-122*).

Despite extensive research demonstrating that epigenetic regulation of gene expression is essential for mammalian development (*22, 23, 25*), how loss of epigenetic regulation in humans contributes to structural malformations remains unclear. Mutations in genes that encode chromatin modifiers have been reported in patients with neurodevelopmental diseases and in diseases that occur later in life (*27-32, 123*). Furthermore, defects in epigenetic gene regulation have been implicated in the mechanisms underlying congenital heart disease and neural tube defects (*24, 33-36*); however, mutations in genes that encode chromatin modifiers are not common among the genes identified in large whole exome or whole genome sequencing in patients with structural malformations (*124, 125*). This may be because epigenetic regulation is ubiquitously necessary during development and therefore any significant disruption of these mechanisms, including loss of a critical co-factor, does not permit embryonic development.

Pathogenic sequence variants in *SIN3A* have been identified in patients with Witteveen-Kolk syndrome (OMIM 613406) with characteristic intellectual disability, growth and feeding difficulties (*92-94, 96*). In this study, 2 patients with CDH were found to have sequence variants in the *SIN3A* gene (Figure 1A). The genetic or epigenetic mechanisms responsible for the difference in the phenotypes in these patients is unclear. The identification of *LONP1* sequence variants in patients with CDH demonstrates that subtle differences in the variants themselves can have a profound impact on the patient phenotype with CDH in some patients and CODAS syndrome in others with cerebral, ocular, dental, auricular, and skeletal anomalies as described previously in patients with *LONP1* gene variants (*15, 126*). The development of modeling approaches that incorporate sequence and chromosomal structural variation and the potential functional consequences of these variants will be essential to accurately predict disease phenotype and penetrance as well as more subtle changes that impact disease severity.

In the developing lung epithelium, SIN3A was shown to be required for cell cycling and branching morphogenesis (*89*). Abnormalities in lung branching have been reported in patients with CDH (*127-129*); however, the more common phenotypes associated with CDH include severe pulmonary hypertension and an overall reduction in lung development causing lung hypoplasia (*128, 130-132*). Abnormalities in alveolar development are also common among patients with CDH (*128*). In the epithelium, deletion of SIN3A led to cell cycle arrest, increased G1 to S-phase checkpoint activity, increased DNA damage, and increased senescence associated beta galactosidase staining (*89*). SIN3A has been associated with regulation of cell cycling and loss of SIN3A has been demonstrated to result in activation of p53 making senescence a likely subsequent loss-of-function phenotype (*70, 133, 134*). In adult type II alveolar epithelial cells, loss of SIN3A resulted in p53 dependent activation of senescence and fibrosis (*90*). In this study, we investigated gene expression changes associated with senescence and found that, although failure of cell cycling and DNA damage were evident in *Sin3a* CKO mice, other changes in gene expression associated with senescence were less clear with both increased and decreased expression of genes implicated in senescence. Although senescence is a likely downstream phenotype following the loss of SIN3A with accumulation of undifferentiated mesenchymal progenitor cells, cell cycle arrest, and DNA damage, our data suggest that the underlying mechanism responsible for this phenotype is loss of SIN3/HDAC regulation of gene expression.

Identifying fetal interventions that improve the outcome of patients with structural malformations is a major objective, especially for CDH (*135-140*). Fetal surgical interventions focus on addressing mechanical compression that occurs in patients with CDH to increase space in the thorax for lung and pulmonary vascular development. Fetal endoscopic tracheal occlusion (FETO) was recently demonstrated to improve survival in patients with severe CDH; however, it

is an invasive procedure associated with increased incidence of preterm delivery (*141, 142*). Preclinical studies have been used to investigate fetal pharmacological interventions that promote lung or pulmonary vascular development and reduce pulmonary hypertension (*135, 136*). Fetal treatment with sildenafil is one of several examples that demonstrate this rationale with promising results (*136, 143-148*); however, concerns have been raised regarding an increase in neonatal pulmonary hypertension in a clinical trial of sildenafil treatment for fetal growth restriction (*149, 150*). Recently, amniotic fluid stem cell-derived extracellular vesicles were shown to improve lung and pulmonary vascular development in a nitrofen-induced rodent model of CDH (*135*). If this approach will be effective in patients where the underlying mechanisms responsible for lung hypoplasia and pulmonary hypertension are multifactorial and heterogeneous is not clear. To better guide fetal surgical, pharmacological, and stem cell-derived interventions for CDH, it is essential to determine which group of patients is likely to respond to each of these approaches.

Genomic analysis, including fetal exome or genome sequencing, would be a useful method to identify patients likely to respond to fetal interventions. CDH has been demonstrated to be a genetically heterogeneous disease and this genetic heterogeneity may be responsible for the wide range of clinical severity in patients with CDH (*11-15*). CDH associated sequence and copy number variants continue to be identified and therefore, at this time, exome and whole genome sequencing are more likely yield a genetic diagnosis than a CDH-specific gene panel. Furthermore, while gene damaging variants have been reported more frequently in patients with complex CDH (*12, 151*), patients with isolated CDH have also a significant burden of likely pathogenic genomic variants (*15, 152*). Our hypothesis is that with an increasing number of CDH patients undergoing genomic analysis we will establish a clear pattern of gene variants and

associated molecular pathway defects that are common in patients with both complex and isolated forms of the disease.

Making a genetic diagnosis in patients with CDH and determining which genetic variants only impact diaphragm development would help identify patients more likely to respond to fetal surgical interventions because the lung and pulmonary vascular defects in these patients are more likely to be due to mechanical compression alone. In contrast, determining which genetic variants play a direct role in lung or pulmonary vascular development, as demonstrated in the case of SIN3A, would help identify patients who are less likely to respond to a treatment focused on mechanical compression alone. These patients are more likely to have primary defects in lung and pulmonary vascular development and are more likely to have lung hypoplasia and pulmonary hypertension that is not responsive to conventional treatment.

In addition to its role in embryonic lung development, SIN3A was recently implicated in the molecular mechanisms responsible for pulmonary hypertension by epigenetic regulation of BMPR2 expression (*153*). Adult patients with pulmonary hypertension were found to have decreased expression of *SIN3A* which was associated with an increased methylation of the *BMPR2* gene promoter and decreased *BMPR2* expression in pulmonary vascular smooth muscle cells (*153*). In this case, intratracheal SIN3A protein administration was used to decrease pulmonary hypertension by decreasing pulmonary artery pressure and restoring normal *Bmpr2* expression in a rat model of pulmonary hypertension (*153*). This work demonstrates the role of SIN3A in adults with pulmonary hypertension and complements our findings that loss of SIN3A resulted in developmental defects in lung and pulmonary vascular development as well as pulmonary hypertension, the major cause of mortality in patients with CDH. These examples demonstrate that further investigation regarding the underlying mechanisms responsible for

abnormal lung and pulmonary vascular development will help identify treatment approaches that target disrupted molecular pathways resulting from the genetic variants present in patients. Genetic analysis in patients with complex structural malformations like CDH will not only help better sub-categorize patients and improve accuracy of prognosis, it will also improve outcomes by permitting individualized and more effective treatment.

MATERIALS AND METHODS

Human genomic analysis

Blood and saliva samples from 827 patient and family trios enrolled in the Diaphragmatic Hernia Research & Exploration; Advancing Molecular Science (DHREAMS) study (http://www.cdhgenetics.com/) were analyzed by whole genome and exome sequencing as described previously (*15, 97*). Signed, informed consent was obtained from participants, and all studies were approved by the institutional review board at each participating institution and the Columbia University Irving Medical Center Institutional Review Board (IRB). Clinical data from medical records were prospectively collected and entered in a central Research Electronic Data Capture (REDCap) database.

Similar to the epidemiological data reported previously for patients with CDH (*2-4*), 59% of this cohort were male and 33.5% had complex CDH with additional anomalies including congenital heart disease, neurodevelopmental disorders, skeletal anomalies, genitourinary anomalies, and gastrointestinal anomalies (*15*). A full description of the methods used for patient and control sequencing analysis, sequence variant confirmation, and the impact of sequence variants on gene transcript or protein structure or function were published previously (*15, 97*).

Animal handling and genetics

Mice were housed and handled according to an animal care committee approved protocol. All experimental procedures were performed in an American Association for Accreditation of Laboratory Animal Care–accredited laboratory animal facility. All mice were bred on a mixed genetic background, and age-matched littermates were used as controls for comparison.

Recombination of the *Sin3a* flox allele (*70*) was achieved by crossing with the previously described *Pax3-cre* (Jax: 005549 (*156*)), *Prx1-cre* (Jax: 005584 (*157*)), or *Tbx4-rtTA; Tet-o-Cre* alleles (*158*). *Tbx4-rtTA* was induced by feeding pregnant mice doxycycline (Teklad) starting at E6.5 or E12.5. *Cre*-positive, *Sin3a*-heterogenous littermates were used as controls.

Histology

Embryonic and early postnatal lungs (<P3) were fixed in 4% paraformaldehyde (PFA). Postnatal lungs (≥ P3) were fix inflated with 4% paraformaldehyde (PFA) by gravity inflation at 20 cm H_2O pressure. Lungs were then processed for paraffin (8μm) or cryo- (10μm, 60μm) sectioning. For each immunofluorescent staining experiment, four control and four *Sin3a* CKO lung sections were analyzed the from middle of each lung. For mean linear intercept analysis, four control and four *Sin3a* CKO lung sections were imaged and analyzed from the apex, middle, and base of the lung.

Mean linear intercept analysis

The mean linear intercept (MLI) of control and *Sin3a* CKO lungs was determined using 20x H&E-stained images. Four mice from each group were analyzed, with four images taken at the apex, middle, and base of each lung. The MLI was calculated using a grid with 14 horizontal lines of a fixed length (450 μm) as described in Branchfield et al, 2016 (*159*). The average MLI was calculated by taking the average for each mouse, then averaged within each group. The reported data are the average MLI for each group with statistical comparison made by unpaired *t*-test.

Immunofluorescence staining

Sections of E16, P0, and P3 lungs were immunostained following standard protocols that consist of deparaffinization, antigen retrieval, and incubation with primary and secondary antibodies. Each experiment was performed a minimum of twice on four controls and four *Sin3a* CKO sectioned lungs. Primary and secondary antibodies used for immunofluorescence staining are listed in Supplemental Table 1.

Pulmonary hypertension assays

Transthoracic echocardiography was performed by the Cardiovascular Physiology Core at the University of Wisconsin-Madison.

To evaluate right ventricular hypertrophy, right ventricular wall thickness (RVWT) was measured by end-diastolic RV diameter, as well as anterior and posterior wall thickness in four control and four *Sin3a* CKO mice at P28. These measurements were collected from M-mode images using the leading edge-to-leading edge convention and normalized to mouse body weight. The reported data are the average right ventricular wall thickness to body weight ratio (RVWT/BW) for each group with statistical comparison made by unpaired *t*-test.

To assess right ventricular function, tricuspid annular plane systolic excursion (TAPSE) was measured in four control and four *Sin3a* CKO mice at P28. The reported data are the average TAPSE for each group with statistical comparison made by unpaired *t*-test.

Direct RV pressure measurements were made during systole by insertion of a 1.0-Fr high-fidelity pressure catheter (Millar Inc.) into the right ventricle of four control and three *Sin3a* CKO mice at P28. Pressure tracings were recorded and analyzed using Notocord. The reported

data are the average right ventricular peak systolic pressure (RVSP) for each group with statistical comparison made by unpaired *t*-test.

Lung mesenchymal cell, endothelial cell, and alveolar epithelial cell quantification

Recombined mesenchymal cell percent: To quantify the percentage of recombined lung mesenchymal cells present in control and Sin3a CKO mice, a *Cre*-responsive red fluorescence reporter allele (ROSA tdTomato Jax: 007914) was crossed into the *Sin3a* conditional deletion genetic cross. Immunofluorescence staining for RFP was performed on paraffin-embedded lung sections (8μm) from four control and four *Sin3a* CKO littermates at P0 and imaged using a 40x objective. The percentage of recombined lung mesenchymal cells was determined by counting the number of RFP positive cells and dividing by the number of DAPI-stained nuclei. The reported data are the average percent of recombined lung mesenchymal cells for each group with statistical comparison made by unpaired *t*-test.

Myofibroblast cell percent: To quantify the number of alveolar myofibroblast precursor cells, a previously described PDGFRa-GFP allele (Jax: 007669, (*160*) was bred into the *Sin3a* conditional deletion genetic cross. Immunofluorescence staining for GFP was performed on paraffin-embedded lung sections (8μm) from four control and four *Sin3a* CKO littermates at P0 and imaged using a 40x objective. The percentage of GFP-positive alveolar myofibroblast precursor cells was determined by counting the number of GFP positive cells and dividing by the number of DAPI-stained nuclei. The reported data are the average percent of GFP-positive cells for each group with statistical comparison made by unpaired *t*-test.

Extracellular matrix analysis: To analyze ECM, immunofluorescence staining for TROPOELASTIN was performed on OCT-embedded lung sections (60μm) from four control

and four *Sin3a* CKO littermates at P3 and imaged on a Leica Sp8 confocal microscope using a 40x objective. TROPOELASTIN staining analysis was conducted on maximal projection z-stacks (40 stacks) from each sample using ImageJ.

Lipofibroblast quantification: To quantify the number of lipofibroblasts, immunofluorescence staining for ADFP was performed on paraffin-embedded lung sections (8μm) from four control and four *Sin3a* CKO littermates at P0 and imaged using a 40x objective. ADFP-positive particles were analyzed in ImageJ (particle size: 0.03-3.05 μm^2) using the threshold and analyze particle tools. The number of ADFP-positive particles was divided by the number of manually counted DAPI-stained nuclei. The reported data are the average ADFP particle ratio for each group with statistical comparison made by unpaired *t*-test.

Endothelial and alveolar epithelial cell analysis: Immunofluorescence staining for ERG, SPC, and HOPEX was used to determine the number of endothelial cells and alveolar type I and II epithelial cells. Paraffin-embedded lung sections (8μm) from four control and four *Sin3a* CKO littermates at P0 were stained and imaged using a 40x objective. The percentage of endothelial, alveolar type I and II epithelial cells was calculated by counting the number of ERG, SPC, and HOPEX-positive cells and dividing by the number of DAPI-stained nuclei. The reported data are the average percent of ERG, SPC, and HOPEX-positive cells for each group with statistical comparisons made by unpaired *t*-test.

Cell proliferation, apoptosis, and DNA damage assays

Cell division: To quantify the number of dividing cells, immunofluorescence for phosphohistone H3 (PHH3) was conducted on paraffin-embedded lung sections (8μm) from four control and four *Sin3a* CKO littermates at E16 and imaged using a 40x objective. The percentage of cells

undergoing cell division was determined by counting the number of PHH3-positive cells and dividing by the number of DAPI nuclei. The reported data are the average percent of PHH3-positive cells for each group with statistical comparison made by unpaired *t*-test.

G1 to S-phase transition: EDU was used to quantify cells undergoing G1 to S-phase transition according to the Click-iT EDU Alexa Fluor 488 Imaging Kit protocol (Invitrogen, Thermo Fisher Scientific). Pregnant mice were injected with EDU 60 minutes prior to euthanasia and tissue collection. Paraffin-embedded lung sections (8μm) from four control and four *Sin3a* CKO littermates at E16 were stained and imaged using a 40x objective. The percentage of cells transitioning from G1 to S-phase was determined by counting the number of EDU-positive cells and dividing by the number of DAPI nuclei. The reported data are the average percent of EDU-positive cells for each group with statistical comparison made by unpaired *t*-test.

Apoptosis: To determine the number of cells undergoing apoptosis, immunofluorescence staining for cleaved caspsase-3 (CC3) was performed on paraffin-embedded lung sections (8μm) from four control and four *Sin3a* CKO littermates at E16 using a 40x objective. The percentage of cells undergoing apoptosis is calculated by counting the number of CC3-positive cells and dividing by the number of DAPI nuclei. The reported data are the average percent of CC3-positive cells for each group with statistical comparison made by unpaired *t*-test.

DNA damage: To identify DNA damage, immunofluorescence staining for H2AX was performed on paraffin-embedded lung sections (8μm) from four control and four *Sin3a* CKO littermates at E16 and imaged using a 40x objective. The percentage of DNA damage was determined by counting the total number of H2AX-positive cells and dividing by the number of DAPI-stained nuclei. The reported data are the average percent of H2AX positive cells for each group with statistical comparison made by unpaired *t*-test.

qRT PCR analysis

Lungs from E16 control and *Sin3a* CKO littermates were homogenized in TRIzol (Thermo Fisher Scientific), and RNA was isolated using the RNeasy Plus Mini Kit (QIAGEN). cDNA was made using the Superscript III First-Strand Synthesis System (Invitrogen, Thermo Fisher Scientific). All qRT-PCR experiments were conducted using 3 biological and 3 technical replicates. qRT-PCR was quantified using the SYBR green (Applied Biosystems, Bio-Rad) and run on a LightCycler 480 (Roche) and a CFX Connect System (Bio-Rad). Gene expression was normalized to β-actin. These reported data are the relative expression normalized to controls with statistical comparison made by unpaired *t*-test. Primers used for qPCR analysis are listed in Supplemental Table 2.

Fluorescent activated cell sorting

Fluorescent activated cell sorting (FACS) was performed by the Flow Cytometry Laboratory at the University of Wisconsin-Madison.

To analyze lung mesenchymal cells that underwent recombination directed by *Tbx4-rtTA; Tet-o-Cre*, FACS was used to sort and collect RFP-labeled cells from E16 *Sin3a* CKO and control lungs. Lungs were digested in collagenase/dispase (Sigma, SKU: 10269638001) for 30 minutes at 37C. After addition of DNase (New England Biolabs, Catalog# M0303S), each sample was filtered through a 40μm filter, followed by three washes with 10% FBS/RPMI media. Pellets were resuspended in red blood cell (RBC) lysis buffer and washed in 10% FBS/RPMI. Immediately prior to sorting, cells were resuspended in FACS buffer with DAPI (1:5,000) and RNasin (1:40, Promega, Catalog# PRN2611). Forward and side scatter plots were

gated to include live, RFP-positive cells. RFP-positive lung mesenchymal cells from control and *Sin3a* CKO mice were sorted into tubes containing 200μL fetal bovine serum using the BioBubble Aria Cell Sorter.

Bulk lung RNA-sequencing, sorted lung mesenchymal cell RNA-sequencing, and sorted lung mesenchymal cell single cell RNA-sequencing

Library preparation and sequencing were performed by the University of Wisconsin-Madison Gene Expression Center and raw reads were processed by the Bioinformatics Center.

Bulk lung RNA-seq: RNA was extracted from whole lungs of four control and four *Sin3a* CKO mice at E16, P0, and P3. Lungs were homogenized in TRIzol (Thermo Fisher Scientific), and RNA was purified using the RNeasy Plus Mini Kit (QIAGEN) and analyzed using the Agilent Bioanalyzer RNA kit. cDNA libraries were made for samples at each stage using Illumina TrueSeq RNA Library Prep Kit (Illumina) and sequenced on the NovaSeq6000 (Illumina). Alignment of 2x150 bp strand-specific Illumina reads to the *Mus musculus* genome was achieved with the STAR v2.5.3a software (*161*). Expression estimation was performed with RSEM v1.3.0 (*162*) and differential gene expression among individual group contrasts was inputted into edgeR (*163*). Statistical significance was adjusted with a Benjamin-Hochberg FDR correction at the 5% level.

Recombined lung mesenchymal cell RNA-seq: Tomato/RFP-positive lung mesenchymal cells sorted by FACS from four control and four *Sin3a* CKO littermates at E16 were homogenized in TRIzol (Thermo Fisher Scientific), and RNA was isolated using the TRIzol RNA extraction protocol. To meet quality standards for sequencing, RNA was cleaned with ethanol and sodium acetate for 30 minutes at -80C.

RNA analysis, cDNA library preparation, sequencing, and analysis: RNA quality was analyzed using the Agilent Bioanalyzer kit. cDNA libraries were made for each sample using the Takara SMARTer RNA v4 with NexteraXT Library Prep Kit (TakaraBio) and sequenced on the NovaSeq6000 (Illumina). Strand-specific Illumina reads were aligned to the *Mus musculus* genome with the STAR v2.5.3a software (*161*). Expression estimation was performed with RSEM v1.3.0 (*162*) and differential gene expression among individual group contrasts was inputted into edgeR (*163*). Statistical significance was adjusted with a Benjamin-Hochberg FDR correction at the 5% level. Heatmaps were generated using normalized gene expression percent in Prism.

Recombined lung mesenchymal cell single cell RNA-seq: FACS sorted Tomato/RFP-positive lung mesenchymal cells from two control and two *Sin3a* CKO littermates at E16 were submitted for 10x Genomics single cell RNA sequencing. mRNA from single lung mesenchymal cells was reverse transcribed to complementary DNA (cDNA) and amplified for each sample and libraries were prepared for sequencing using the 10x Genomics Single Cell 3' v3.1 Regents Kit (10x Genomics, Pleasanton, CA, USA). Cellular suspensions were loaded on a Chromium Controller instrument (10x Genomics) to generate single-cell Gel Bead-In-Emulsions (GEMs). GEM-reverse transcription (RT) was performed in an Eppendorf Mastercycler Pro thermal cycler (Eppendorf, Enfield, CT, USA). GEMs were collected and the cDNA was amplified and purified with SPRIselect Reagent kit (Beckman Coulter, Brea, CA, USA). cDNA was analyzed on an Agilent Bioanalyzer High Sensitivity chip (Agilent Technologies, Santa Clara, CA, USA). Dual indexed sequencing libraries were constructed using Chromium Single-Cell 3' Library Construction Kit for enzymatic fragmentation, end-repair, A-tailing, adapter ligation, ligation cleanup, sample index PCR, and PCR cleanup. The barcoded sequencing libraries were

quantified using Qubit high sensitivity DNA reagents (Invitrogen Qubit, Thermo Fisher Scientific, Waltham, MA, USA) and analyzed on an Agilent Bioanalyzer DNA 1000 chip. Sequencing libraries were loaded on a NextSeq 6000 with an S1 flow cell (Next seq info) and sequenced to a depth of 35,000 reads per cell.

10x scRNA-seq alignment and gene quantification: Cell Ranger Toolkit v6.1.1 was used to align reads and generate gene-cell UMI matrices for the two control and two *Sin3a* CKO biological replicates using mouse genome GRCm38 and Ensembl gene annotations v102. The outputs of Cell Ranger count for all samples were aggregated using Cell Ranger aggr. Spliced and unspliced count matrices for scvelo analyses were generated using velocyto v0.17.17.

10x scRNA-seq quality control, integration, clustering, cluster annotation: R v4.0.2 and Seurat v4.0.5 were used for the integration and analysis of scRNA-seq samples (*164*). Aggregate gene-cell expression matrix was filtered to keep genes expressed in at least 3 cells and cells with a minimum of 200 detected genes for downstream analysis. Low quality cells and potential doublets were removed by filtering cells with <200 or >600 detected genes and mitochondrial content of >10%. The four biological replicates (two controls and two *Sin3a* CKOs) were integrated using the SCTranform method according to Seurat vignette (https://satijalab.org/seurat/articles/integration_introduction.html#performing-integration-on-datasets-normalized-with-sctransform-1) and selecting for 3000 variable genes. After integration, the default assay was set to 'RNA' and the UMI matrix was normalized using 'NormalizeData' for cluster marker identification, differential analysis (DE), and gene expression visualizations. Cluster markers were identified using only the control sample replicates by applying 'FindAllMarkers' function. Cluster assignment was conducted by identifying strongly and uniquely expressed marker genes (expressed by greater than 90% of cells within the cluster and

less than 30% of cells outside the cluster) in previously reported embryonic mouse lung mesenchymal cells (*99, 165*). The number of cells identified within each cluster was reported for each mouse. Analysis of the distribution of recombined lung mesenchymal cells was performed by comparing the percentage of cells within each cluster in *Sin3a* CKO mice to the percentage of cells within each cluster in control mice with statistical comparison made by χ^2 test.

10x scRNA-seq pathway, differential gene expression, and RNA velocity analyses: Differentially expressed (DE) genes between *Sin3a* CKO and control lung mesenchymal cells for each cluster were identified using 'FindMarkers' functions and 'MAST' statistical framework. Pathway analysis of the DE gene lists were performed using Ingenuity Pathway Analysis (Qiagen, Redwood City, USA). RNA velocity analyses were performed using scvelo v0.2.4 according to instructions from the official scvelo documentation (https://scvelo.readthedocs.io/VelocityBasics/) (*100*). Analysis of the RNA velocity length was conducted by comparing the RNA velocity lengths observed in each cluster in *Sin3a* CKO mice to those observed in each cluster in control mice with statistical comparison made by Z-test.

Embryonic histone acetyltransferase and histone deacetylase inhibition assays

Anacardic acid (AA) (Calbiochem-Sigma Aldrich, CAS 16611-84-0), A-485 (Tocris, Catalog# 6387), and Trichostatin A (TSA) (Sigma Aldrich, CAS Number: 58880-19-6) were used to treat control and *Sin3a* CKO littermate embryos via intraperitoneal injection of pregnant dams. These experiments were compared to vehicle (DMSO) control treated control and *Sin3a* CKO embryos.

G1 to S-phase transition and DNA damage analysis: Pregnant mice were treated daily with anacardic acid (5mg/kg), A-485 (5mg/kg), or TSA (16mg/kg) from E12-16. At E16, lungs were harvested and fixed in 4% PFA. To quantify G1 to S-phase transitioning cells and DNA damage,

immunofluorescence staining for EDU and H2AX was performed on paraffin-embedded lung sections (8μm) from four control and four *Sin3a* CKO littermates at E16 and imaged using a 40x objective. The percentage cells undergoing G1 to S-phase transition and percent DNA damage was calculated by counting the number of EDU-positive or H2AX-positive cells divided by the number of DAPI-stained nuclei. The reported data are the average percent of EDU- or H2AX-positive cells with and without treatment for each group. Statistical comparisons were made using 1-way ANOVA.

Alveolar myofibroblast and lung simplification rescue: Pregnant mice were treated daily with AA (5mg/kg), from E12-16. Lungs were harvested at P0 and fixed in 4% PFA. To quantify the number of PDGFRa alveolar myofibroblast precursor cells, immunofluorescence staining for GFP was performed on paraffin-embedded lung sections (8μm) from four control and four *Sin3a* CKO littermates at P0 and imaged using a 40x objective. The percentage of GFP-positive alveolar myofibroblasts was determined by counting the number of GFP-positive cells and dividing by the number of DAPI-stained nuclei. The reported data are the average percent of GFP-positive cells with or without treatment for each group. Statistical comparisons were made using 1-way ANOVA.

To assess lung simplification, the MLI of four AA-treated control and AA-treated *Sin3a* CKO lungs P0 was determined at P0 using 20x H&E-stained images. Four mice from each group were analyzed with four images taken at the apex, middle, and base of the lung. The MLI was calculated using a grid with 14 horizontal lines of a fixed length (450 μm) as described in Branchfield et al, 2016 (*159*). The average MLI was calculated by calculating the average for each mouse, then averaged within each group. The reported data are the average MLI for each group with statistical comparisons made by 1-way ANOVA.

LIST OF SUPPLEMENTARY MATERIALS

REFERENCES AND NOTES

1. *Mortality in the United States, 2019* (2020 https://www.cdc.gov/nchs/data/databriefs/db395-H.pdf).

2. J. Balayla, H. A. Abenhaim, Incidence, predictors and outcomes of congenital diaphragmatic hernia: a population-based study of 32 million births in the United States. *J Matern Fetal Neonatal Med* **27**, 1438-1444 (2014).

3. M. R. McGivern *et al.*, Epidemiology of congenital diaphragmatic hernia in Europe: a register-based study. *Arch Dis Child Fetal Neonatal Ed* **100**, F137-144 (2015).

4. M. Paoletti *et al.*, Prevalence and risk factors for congenital diaphragmatic hernia: A global view. *J Pediatr Surg* **55**, 2297-2307 (2020).

5. H. Aly, D. Bianco-Batlles, M. A. Mohamed, T. A. Hammad, Mortality in infants with congenital diaphragmatic hernia: a study of the United States National Database. *J Perinatol* **30**, 553-557 (2010).

6. S. L. Carmichael *et al.*, Survival of infants with congenital diaphragmatic hernia in California: impact of hospital, clinical, and sociodemographic factors. *J Perinatol* **40**, 943-951 (2020).

7. M. D. Politis *et al.*, Prevalence and mortality in children with congenital diaphragmatic hernia: a multicountry study. *Ann Epidemiol* **56**, 61-69.e63 (2021).

8. R. Ramakrishnan *et al.*, Trends, correlates, and survival of infants with congenital diaphragmatic hernia and its subtypes. *Birth Defects Res* **110**, 1107-1117 (2018).

9. J. Wynn *et al.*, Outcomes of congenital diaphragmatic hernia in the modern era of management. *J Pediatr* **163**, 114-119.e111 (2013).

10. R. B. Seabrook *et al.*, Treatment of pulmonary hypertension during initial hospitalization in a multicenter cohort of infants with congenital diaphragmatic hernia (CDH). *J Perinatol* **41**, 803-813 (2021).

11. E. L. Bogenschutz *et al.*, Deep whole-genome sequencing of multiple proband tissues and parental blood reveals the complex genetic etiology of congenital diaphragmatic hernias. *HGG Adv* **1**, (2020).

12. M. Longoni *et al.*, Genome-wide enrichment of damaging de novo variants in patients with isolated and complex congenital diaphragmatic hernia. *Hum Genet* **136**, 679-691 (2017).

13. M. Kammoun *et al.*, Genetic profile of isolated congenital diaphragmatic hernia revealed by targeted next-generation sequencing. *Prenat Diagn* **38**, 654-663 (2018).

14. H. Qi *et al.*, De novo variants in congenital diaphragmatic hernia identify MYRF as a new syndrome and reveal genetic overlaps with other developmental disorders. *PLoS Genet* **14**, e1007822 (2018).

15. L. Qiao *et al.*, Rare and de novo variants in 827 congenital diaphragmatic hernia probands implicate LONP1 as candidate risk gene. *Am J Hum Genet* **108**, 1964-1980 (2021).

16. A. J. Merrell *et al.*, Muscle connective tissue controls development of the diaphragm and is a source of congenital diaphragmatic hernias. *Nat Genet* **47**, 496-504 (2015).

17. K. G. Ackerman *et al.*, Gata4 is necessary for normal pulmonary lobar development. *Am J Respir Cell Mol Biol* **36**, 391-397 (2007).

18. K. G. Ackerman *et al.*, Fog2 is required for normal diaphragm and lung development in mice and humans. *PLoS Genet* **1**, 58-65 (2005).

19. M. K. Russell *et al.*, Congenital diaphragmatic hernia candidate genes derived from embryonic transcriptomes. *Proc Natl Acad Sci U S A* **109**, 2978-2983 (2012).

20. R. Carmona *et al.*, Conditional deletion of WT1 in the septum transversum mesenchyme causes congenital diaphragmatic hernia in mice. *Elife* **5**, (2016).

21. D. J. McCulley *et al.*, PBX transcription factors drive pulmonary vascular adaptation to birth. *J Clin Invest* **128**, 655-667 (2018).

22. J. Wu *et al.*, Chromatin analysis in human early development reveals epigenetic transition during ZGA. *Nature* **557**, 256-260 (2018).

23. F. Santos, B. Hendrich, W. Reik, W. Dean, Dynamic reprogramming of DNA methylation in the early mouse embryo. *Dev Biol* **241**, 172-182 (2002).

24. R. Gilsbach *et al.*, Distinct epigenetic programs regulate cardiac myocyte development and disease in the human heart in vivo. *Nat Commun* **9**, 391 (2018).

25. Y. Wang *et al.*, Single-cell multiomics sequencing reveals the functional regulatory landscape of early embryos. *Nat Commun* **12**, 1247 (2021).

26. E. Rexhaj *et al.*, Fetal programming of pulmonary vascular dysfunction in mice: role of epigenetic mechanisms. *Am J Physiol Heart Circ Physiol* **301**, H247-252 (2011).

27. R. E. Amir *et al.*, Rett syndrome is caused by mutations in X-linked MECP2, encoding methyl-CpG-binding protein 2. *Nat Genet* **23**, 185-188 (1999).

28. H. Shirohzu *et al.*, Three novel DNMT3B mutations in Japanese patients with ICF syndrome. *Am J Med Genet* **112**, 31-37 (2002).

29. S. Timmermann, H. Lehrmann, A. Polesskaya, A. Harel-Bellan, Histone acetylation and disease. *Cell Mol Life Sci* **58**, 728-736 (2001).

30. S. Ropero *et al.*, A truncating mutation of HDAC2 in human cancers confers resistance to histone deacetylase inhibition. *Nat Genet* **38**, 566-569 (2006).

31. K. S. Cho, L. I. Elizondo, C. F. Boerkoel, Advances in chromatin remodeling and human disease. *Curr Opin Genet Dev* **14**, 308-315 (2004).

32. E. Brookes, Y. Shi, Diverse epigenetic mechanisms of human disease. *Annu Rev Genet* **48**, 237-268 (2014).

33. N. D. Greene, P. Stanier, G. E. Moore, The emerging role of epigenetic mechanisms in the etiology of neural tube defects. *Epigenetics* **6**, 875-883 (2011).

34. S. Zaidi *et al.*, De novo mutations in histone-modifying genes in congenital heart disease. *Nature* **498**, 220-223 (2013).

35. J. Cao *et al.*, The role of DNA methylation in syndromic and non-syndromic congenital heart disease. *Clin Epigenetics* **13**, 93 (2021).

36. S. Chowdhury *et al.*, Maternal genome-wide DNA methylation patterns and congenital heart defects. *PLoS One* **6**, e16506 (2011).

37. E. Li, T. H. Bestor, R. Jaenisch, Targeted mutation of the DNA methyltransferase gene results in embryonic lethality. *Cell* **69**, 915-926 (1992).

38. M. Okano, D. W. Bell, D. A. Haber, E. Li, DNA methyltransferases Dnmt3a and Dnmt3b are essential for de novo methylation and mammalian development. *Cell* **99**, 247-257 (1999).

39. G. Lagger *et al.*, Essential function of histone deacetylase 1 in proliferation control and CDK inhibitor repression. *EMBO J* **21**, 2672-2681 (2002).

40. R. L. Montgomery *et al.*, Histone deacetylases 1 and 2 redundantly regulate cardiac morphogenesis, growth, and contractility. *Genes Dev* **21**, 1790-1802 (2007).

41. Y. Wang *et al.*, Development and regeneration of Sox2+ endoderm progenitors are regulated by a Hdac1/2-Bmp4/Rb1 regulatory pathway. *Dev Cell* **24**, 345-358 (2013).

42. Y. Wang *et al.*, HDAC3-Dependent Epigenetic Pathway Controls Lung Alveolar Epithelial Cell Remodeling and Spreading via miR-17-92 and TGF-β Signaling Regulation. *Dev Cell* **36**, 303-315 (2016).

43. J. S. Hagood, Beyond the genome: epigenetic mechanisms in lung remodeling. *Physiology (Bethesda)* **29**, 177-185 (2014).

44. K. Ito *et al.*, Decreased histone deacetylase activity in chronic obstructive pulmonary disease. *N Engl J Med* **352**, 1967-1976 (2005).

45. K. Ito *et al.*, Expression and activity of histone deacetylases in human asthmatic airways. *Am J Respir Crit Care Med* **166**, 392-396 (2002).

46. B. G. Cosío *et al.*, Histone acetylase and deacetylase activity in alveolar macrophages and blood mononocytes in asthma. *Am J Respir Crit Care Med* **170**, 141-147 (2004).

47. M. Li, Y. Zheng, H. Yuan, Y. Liu, X. Wen, Effects of dynamic changes in histone acetylation and deacetylase activity on pulmonary fibrosis. *Int Immunopharmacol* **52**, 272-280 (2017).

48. C. M. Robinson, R. Neary, A. Levendale, C. J. Watson, J. A. Baugh, Hypoxia-induced DNA hypermethylation in human pulmonary fibroblasts is associated with Thy-1 promoter methylation and the development of a pro-fibrotic phenotype. *Respir Res* **13**, 74 (2012).

49. B. Bartling *et al.*, Comparative application of antibody and gene array for expression profiling in human squamous cell lung carcinoma. *Lung Cancer* **49**, 145-154 (2005).

50. Y. Minamiya *et al.*, Strong expression of HDAC3 correlates with a poor prognosis in patients with adenocarcinoma of the lung. *Tumour Biol* **31**, 533-539 (2010).

51. Y. Gan *et al.*, Role of histone deacetylation in cell-specific expression of endothelial nitric-oxide synthase. *J Biol Chem* **280**, 16467-16475 (2005).

52. H. J. Bogaard *et al.*, Suppression of histone deacetylases worsens right ventricular dysfunction after pulmonary artery banding in rats. *Am J Respir Crit Care Med* **183**, 1402-1410 (2011).

53. A. Ruiz-Carrillo, L. J. Wangh, V. G. Allfrey, Processing of newly synthesized histone molecules. *Science* **190**, 117-128 (1975).

54. A. T. Annunziato, R. L. Seale, Histone deacetylation is required for the maturation of newly replicated chromatin. *J Biol Chem* **258**, 12675-12684 (1983).

55. M. H. Kuo, C. D. Allis, Roles of histone acetyltransferases and deacetylases in gene regulation. *Bioessays* **20**, 615-626 (1998).

56. J. H. Lee, S. R. Hart, D. G. Skalnik, Histone deacetylase activity is required for embryonic stem cell differentiation. *Genesis* **38**, 32-38 (2004).

57. M. Haberland, R. L. Montgomery, E. N. Olson, The many roles of histone deacetylases in development and physiology: implications for disease and therapy. *Nat Rev Genet* **10**, 32-42 (2009).

58. B. T. Weinert *et al.*, Time-Resolved Analysis Reveals Rapid Dynamics and Broad Scope of the CBP/p300 Acetylome. *Cell* **174**, 231-244.e212 (2018).

59. R. D. Kelly, S. M. Cowley, The physiological roles of histone deacetylase (HDAC) 1 and 2: complex co-stars with multiple leading parts. *Biochem Soc Trans* **41**, 741-749 (2013).

60. M. Bantscheff *et al.*, Chemoproteomics profiling of HDAC inhibitors reveals selective targeting of HDAC complexes. *Nat Biotechnol* **29**, 255-265 (2011).

61. Y. Zhang *et al.*, Analysis of the NuRD subunits reveals a histone deacetylase core complex and a connection with DNA methylation. *Genes Dev* **13**, 1924-1935 (1999).

62. T. Itoh *et al.*, Structural and functional characterization of a cell cycle associated HDAC1/2 complex reveals the structural basis for complex assembly and nucleosome targeting. *Nucleic Acids Res* **43**, 2033-2044 (2015).

63. G. E. Adams, A. Chandru, S. M. Cowley, Co-repressor, co-activator and general transcription factor: the many faces of the Sin3 histone deacetylase (HDAC) complex. *Biochem J* **475**, 3921-3932 (2018).

64. C. A. Hassig, T. C. Fleischer, A. N. Billin, S. L. Schreiber, D. E. Ayer, Histone deacetylase activity is required for full transcriptional repression by mSin3A. *Cell* **89**, 341-347 (1997).

65. C. D. Laherty *et al.*, Histone deacetylases associated with the mSin3 corepressor mediate mad transcriptional repression. *Cell* **89**, 349-356 (1997).

66. L. Nagy *et al.*, Nuclear receptor repression mediated by a complex containing SMRT, mSin3A, and histone deacetylase. *Cell* **89**, 373-380 (1997).

67. D. Kadosh, K. Struhl, Repression by Ume6 involves recruitment of a complex containing Sin3 corepressor and Rpd3 histone deacetylase to target promoters. *Cell* **89**, 365-371 (1997).

68. Y. Zhang, R. Iratni, H. Erdjument-Bromage, P. Tempst, D. Reinberg, Histone deacetylases and SAP18, a novel polypeptide, are components of a human Sin3 complex. *Cell* **89**, 357-364 (1997).

69. A. Lai *et al.*, RBP1 recruits the mSIN3-histone deacetylase complex to the pocket of retinoblastoma tumor suppressor family proteins found in limited discrete regions of the nucleus at growth arrest. *Mol Cell Biol* **21**, 2918-2932 (2001).

70. J. H. Dannenberg *et al.*, mSin3A corepressor regulates diverse transcriptional networks governing normal and neoplastic growth and survival. *Genes Dev* **19**, 1581-1595 (2005).

71. L. A. Pile, E. M. Schlag, D. A. Wassarman, The SIN3/RPD3 deacetylase complex is essential for G(2) phase cell cycle progression and regulation of SMRTER corepressor levels. *Mol Cell Biol* **22**, 4965-4976 (2002).

72. H. Yoshimoto, M. Ohmae, I. Yamashita, The Saccharomyces cerevisiae GAM2/SIN3 protein plays a role in both activation and repression of transcription. *Mol Gen Genet* **233**, 327-330 (1992).

73. M. Vidal, R. Strich, R. E. Esposito, R. F. Gaber, RPD1 (SIN3/UME4) is required for maximal activation and repression of diverse yeast genes. *Mol Cell Biol* **11**, 6306-6316 (1991).

74. B. E. Bernstein, J. K. Tong, S. L. Schreiber, Genomewide studies of histone deacetylase function in yeast. *Proc Natl Acad Sci U S A* **97**, 13708-13713 (2000).

75. T. K. Das, J. Sangodkar, N. Negre, G. Narla, R. L. Cagan, Sin3a acts through a multi-gene module to regulate invasion in Drosophila and human tumors. *Oncogene* **32**, 3184-3197 (2013).

76. G. A. Baltus, M. P. Kowalski, A. V. Tutter, S. Kadam, A positive regulatory role for the mSin3A-HDAC complex in pluripotency through Nanog and Sox2. *J Biol Chem* **284**, 6998-7006 (2009).

77. L. Icardi *et al.*, The Sin3a repressor complex is a master regulator of STAT transcriptional activity. *Proc Natl Acad Sci U S A* **109**, 12058-12063 (2012).

78. V. V. Baker, H. M. Shingleton, K. D. Hatch, D. M. Miller, Selective inhibition of c-myc expression by the ribonucleic acid synthesis inhibitor mithramycin. *Am J Obstet Gynecol* **158**, 762-767 (1988).

79. R. Kadamb, S. Mittal, N. Bansal, H. Batra, D. Saluja, Sin3: insight into its transcription regulatory functions. *Eur J Cell Biol* **92**, 237-246 (2013).

80. T. P. Neufeld, A. H. Tang, G. M. Rubin, A genetic screen to identify components of the sina signaling pathway in Drosophila eye development. *Genetics* **148**, 277-286 (1998).

81. L. A. Pile, D. A. Wassarman, Chromosomal localization links the SIN3-RPD3 complex to the regulation of chromatin condensation, histone acetylation and gene expression. *EMBO J* **19**, 6131-6140 (2000).

82. V. Sharma, A. Swaminathan, R. Bao, L. A. Pile, Drosophila SIN3 is required at multiple stages of development. *Dev Dyn* **237**, 3040-3050 (2008).

83. G. Pennetta, D. Pauli, The Drosophila Sin3 gene encodes a widely distributed transcription factor essential for embryonic viability. *Dev Genes Evol* **208**, 531-536 (1998).

84. A. Swaminathan, L. A. Pile, Regulation of cell proliferation and wing development by Drosophila SIN3 and String. *Mech Dev* **127**, 96-106 (2010).

85. J. Pellegrino, D. H. Castrillon, G. David, Chromatin associated Sin3A is essential for male germ cell lineage in the mouse. *Dev Biol* **369**, 349-355 (2012).

86. S. M. Cowley *et al.*, The mSin3A chromatin-modifying complex is essential for embryogenesis and T-cell development. *Mol Cell Biol* **25**, 6990-7004 (2005).

87. G. David *et al.*, Specific requirement of the chromatin modifier mSin3B in cell cycle exit and cellular differentiation. *Proc Natl Acad Sci U S A* **105**, 4168-4172 (2008).

88. C. van Oevelen *et al.*, The mammalian Sin3 proteins are required for muscle development and sarcomere specification. *Mol Cell Biol* **30**, 5686-5697 (2010).

89. C. Yao *et al.*, Sin3a regulates epithelial progenitor cell fate during lung development. *Development* **144**, 2618-2628 (2017).

90. C. Yao *et al.*, Senescence of Alveolar Type 2 Cells Drives Progressive Pulmonary Fibrosis. *Am J Respir Crit Care Med* **203**, 707-717 (2021).

91. H. C. Mefford *et al.*, Further clinical and molecular delineation of the 15q24 microdeletion syndrome. *J Med Genet* **49**, 110-118 (2012).

92. Y. Narumi-Kishimoto *et al.*, Novel SIN3A mutation identified in a Japanese patient with Witteveen-Kolk syndrome. *Eur J Med Genet* **62**, 103547 (2019).

93. J. S. Witteveen *et al.*, Haploinsufficiency of MeCP2-interacting transcriptional co-repressor SIN3A causes mild intellectual disability by affecting the development of cortical integrity. *Nat Genet* **48**, 877-887 (2016).

94. L. C. M. van Dongen *et al.*, Behavior and cognitive functioning in Witteveen-Kolk syndrome. *Am J Med Genet A* **182**, 2384-2390 (2020).

95. X. Latypova *et al.*, Haploinsufficiency of the Sin3/HDAC corepressor complex member SIN3B causes a syndromic intellectual disability/autism spectrum disorder. *Am J Hum Genet* **108**, 929-941 (2021).

96. M. Balasubramanian *et al.*, Comprehensive study of 28 individuals with SIN3A-related disorder underscoring the associated mild cognitive and distinctive facial phenotype. *Eur J Hum Genet* **29**, 625-636 (2021).

97. L. Yu *et al.*, De novo copy number variants are associated with congenital diaphragmatic hernia. *J Med Genet* **49**, 650-659 (2012).

98. P. McDonel, J. Demmers, D. W. Tan, F. Watt, B. D. Hendrich, Sin3a is essential for the genome integrity and viability of pluripotent cells. *Dev Biol* **363**, 62-73 (2012).

99. X. Liu *et al.*, Categorization of lung mesenchymal cells in development and fibrosis. *iScience* **24**, 102551 (2021).

100. V. Bergen, M. Lange, S. Peidli, F. A. Wolf, F. J. Theis, Generalizing RNA velocity to transient cell states through dynamical modeling. *Nat Biotechnol* **38**, 1408-1414 (2020).

101. A. Chaubal, L. A. Pile, Same agent, different messages: insight into transcriptional regulation by SIN3 isoforms. *Epigenetics Chromatin* **11**, 17 (2018).

102. F. J. Dekker, T. van den Bosch, N. I. Martin, Small molecule inhibitors of histone acetyltransferases and deacetylases are potential drugs for inflammatory diseases. *Drug Discov Today* **19**, 654-660 (2014).

103. E. Menegola *et al.*, Inhibition of histone deacetylase activity on specific embryonic tissues as a new mechanism for teratogenicity. *Birth Defects Res B Dev Reprod Toxicol* **74**, 392-398 (2005).

104. F. Zhou *et al.*, Selective inhibition of CBP/p300 HAT by A-485 results in suppression of lipogenesis and hepatic gluconeogenesis. *Cell Death Dis* **11**, 745 (2020).

105. C. Peng *et al.*, Inhibition of histone H3K9 acetylation by anacardic acid can correct the over-expression of Gata4 in the hearts of fetal mice exposed to alcohol during pregnancy. *PLoS One* **9**, e104135 (2014).

106. L. Verdone, E. Agricola, M. Caserta, E. Di Mauro, Histone acetylation in gene regulation. *Brief Funct Genomic Proteomic* **5**, 209-221 (2006).

107. L. Verdone, M. Caserta, E. Di Mauro, Role of histone acetylation in the control of gene expression. *Biochem Cell Biol* **83**, 344-353 (2005).

108. K. Struhl, Histone acetylation and transcriptional regulatory mechanisms. *Genes Dev* **12**, 599-606 (1998).

109. A. B. Osipovich, R. Gangula, P. G. Vianna, M. A. Magnuson, Setd5 is essential for mammalian development and the co-transcriptional regulation of histone acetylation. *Development* **143**, 4595-4607 (2016).

110. K. W. McCool, X. Xu, D. B. Singer, F. E. Murdoch, M. K. Fritsch, The role of histone acetylation in regulating early gene expression patterns during early embryonic stem cell differentiation. *J Biol Chem* **282**, 6696-6706 (2007).

111. R. Bar-Ziv, Y. Voichek, N. Barkai, Chromatin dynamics during DNA replication. *Genome Res* **26**, 1245-1256 (2016).

112. A. Unnikrishnan, P. R. Gafken, T. Tsukiyama, Dynamic changes in histone acetylation regulate origins of DNA replication. *Nat Struct Mol Biol* **17**, 430-437 (2010).

113. M. J. Pazin, J. T. Kadonaga, What's up and down with histone deacetylation and transcription? *Cell* **89**, 325-328 (1997).

114. E. Seto, M. Yoshida, Erasers of histone acetylation: the histone deacetylase enzymes. *Cold Spring Harb Perspect Biol* **6**, a018713 (2014).

115. A. Peserico, C. Simone, Physical and functional HAT/HDAC interplay regulates protein acetylation balance. *J Biomed Biotechnol* **2011**, 371832 (2011).

116. L. Haery, R. C. Thompson, T. D. Gilmore, Histone acetyltransferases and histone deacetylases in B- and T-cell development, physiology and malignancy. *Genes Cancer* **6**, 184-213 (2015).

117. L. Legoff, S. C. D'Cruz, S. Tevosian, M. Primig, F. Smagulova, Transgenerational Inheritance of Environmentally Induced Epigenetic Alterations during Mammalian Development. *Cells* **8**, (2019).

118. K. A. Gelato, W. Fischle, Role of histone modifications in defining chromatin structure and function. *Biol Chem* **389**, 353-363 (2008).

119. R. Ramakrishnan *et al.*, Maternal exposure to ambient cadmium levels, maternal smoking during pregnancy, and congenital diaphragmatic hernia. *Birth Defects Res* **111**, 1399-1407 (2019).

120. K. M. Caspers *et al.*, Maternal periconceptional exposure to cigarette smoking and alcohol consumption and congenital diaphragmatic hernia. *Birth Defects Res A Clin Mol Teratol* **88**, 1040-1049 (2010).

121. R. H. Finnell *et al.*, Gene Environment Interactions in the Etiology of Neural Tube Defects. *Front Genet* **12**, 659612 (2021).

122. T. Workalemahu *et al.*, Genetic and Environmental Influences on Fetal Growth Vary during Sensitive Periods in Pregnancy. *Sci Rep* **8**, 7274 (2018).

123. G. W. Santen *et al.*, Mutations in SWI/SNF chromatin remodeling complex gene ARID1B cause Coffin-Siris syndrome. *Nat Genet* **44**, 379-380 (2012).

124. S. Petrovski *et al.*, Whole-exome sequencing in the evaluation of fetal structural anomalies: a prospective cohort study. *Lancet* **393**, 758-767 (2019).

125. J. Lord *et al.*, Prenatal exome sequencing analysis in fetal structural anomalies detected by ultrasonography (PAGE): a cohort study. *Lancet* **393**, 747-757 (2019).

126. K. A. Strauss *et al.*, CODAS syndrome is associated with mutations of LONP1, encoding mitochondrial AAA+ Lon protease. *Am J Hum Genet* **96**, 121-135 (2015).

127. K. Nose *et al.*, Airway anomalies in patients with congenital diaphragmatic hernia. *J Pediatr Surg* **35**, 1562-1565 (2000).

128. D. Ameis, N. Khoshgoo, R. Keijzer, Abnormal lung development in congenital diaphragmatic hernia. *Semin Pediatr Surg* **26**, 123-128 (2017).

129. C. A. Ryan, N. N. Finer, P. C. Etches, A. J. Tierney, A. Peliowski, Congenital diaphragmatic hernia: associated malformations--cystic adenomatoid malformation, extralobular sequestration, and laryngotracheoesophageal cleft: two case reports. *J Pediatr Surg* **30**, 883-885 (1995).

130. D. Kluth *et al.*, The natural history of congenital diaphragmatic hernia and pulmonary hypoplasia in the embryo. *J Pediatr Surg* **28**, 456-462; discussion 462-453 (1993).

131. H. Mohseni-Bod, D. Bohn, Pulmonary hypertension in congenital diaphragmatic hernia. *Semin Pediatr Surg* **16**, 126-133 (2007).

132. B. Thébaud, J. C. Mercier, A. T. Dinh-Xuan, Congenital diaphragmatic hernia. A cause of persistent pulmonary hypertension of the newborn which lacks an effective therapy. *Biol Neonate* **74**, 323-336 (1998).

133. D. S. Wilkinson, W. W. Tsai, M. A. Schumacher, M. C. Barton, Chromatin-bound p53 anchors activated Smads and the mSin3A corepressor to confer transforming-growth-factor-beta-mediated transcription repression. *Mol Cell Biol* **28**, 1988-1998 (2008).

134. J. T. Zilfou, W. H. Hoffman, M. Sank, D. L. George, M. Murphy, The corepressor mSin3a interacts with the proline-rich domain of p53 and protects p53 from proteasome-mediated degradation. *Mol Cell Biol* **21**, 3974-3985 (2001).

135. L. Antounians *et al.*, Fetal lung underdevelopment is rescued by administration of amniotic fluid stem cell extracellular vesicles in rodents. *Sci Transl Med* **13**, (2021).

136. F. Okolo, G. Zhang, J. Rhodes, G. K. Gittes, D. A. Potoka, Intra-Amniotic Sildenafil Treatment Promotes Lung Growth and Attenuates Vascular Remodeling in an Experimental Model of Congenital Diaphragmatic Hernia. *Fetal Diagn Ther*, 1-13 (2020).

137. R. M. Grivell, C. Andersen, J. M. Dodd, Prenatal interventions for congenital diaphragmatic hernia for improving outcomes. *Cochrane Database Syst Rev*, CD008925 (2015).

138. D. S. Mous *et al.*, Treatment of rat congenital diaphragmatic hernia with sildenafil and NS-304, selexipag's active compound, at the pseudoglandular stage improves lung vasculature. *Am J Physiol Lung Cell Mol Physiol* **315**, L276-L285 (2018).

139. C. Jeanty, S. M. Kunisaki, T. C. MacKenzie, Novel non-surgical prenatal approaches to treating congenital diaphragmatic hernia. *Semin Fetal Neonatal Med* **19**, 349-356 (2014).

140. M. A. Verla, C. C. Style, O. O. Olutoye, Prenatal intervention for the management of congenital diaphragmatic hernia. *Pediatr Surg Int* **34**, 579-587 (2018).

141. J. A. Deprest *et al.*, Randomized Trial of Fetal Surgery for Severe Left Diaphragmatic Hernia. *N Engl J Med* **385**, 107-118 (2021).

142. J. A. Deprest *et al.*, Randomized Trial of Fetal Surgery for Moderate Left Diaphragmatic Hernia. *N Engl J Med* **385**, 119-129 (2021).

143. F. M. Russo *et al.*, Transplacental sildenafil rescues lung abnormalities in the rabbit model of diaphragmatic hernia. *Thorax* **71**, 517-525 (2016).

144. A. J. Kashyap *et al.*, Antenatal sildenafil treatment improves neonatal pulmonary hemodynamics and gas exchange in lambs with diaphragmatic hernia. *Ultrasound Obstet Gynecol* **54**, 506-516 (2019).

145. F. M. Russo *et al.*, Complementary Effect of Maternal Sildenafil and Fetal Tracheal Occlusion Improves Lung Development in the Rabbit Model of Congenital Diaphragmatic Hernia. *Ann Surg* **275**, e586-e595 (2022).

146. C. M. Burgos *et al.*, Improved pulmonary function in the nitrofen model of congenital diaphragmatic hernia following prenatal maternal dexamethasone and/or sildenafil. *Pediatr Res* **80**, 577-585 (2016).

147. J. Kattan, C. Céspedes, A. González, C. P. Vio, Sildenafil stimulates and dexamethasone inhibits pulmonary vascular development in congenital diaphragmatic hernia rat lungs. *Neonatology* **106**, 74-80 (2014).

148. C. Luong *et al.*, Antenatal sildenafil treatment attenuates pulmonary hypertension in experimental congenital diaphragmatic hernia. *Circulation* **123**, 2120-2131 (2011).

149. A. Pels *et al.*, Maternal Sildenafil vs Placebo in Pregnant Women With Severe Early-Onset Fetal Growth Restriction: A Randomized Clinical Trial. *JAMA Netw Open* **3**, e205323 (2020).

150. A. Pels *et al.*, Neonatal pulmonary hypertension after severe early-onset fetal growth restriction: post hoc reflections on the Dutch STRIDER study. *Eur J Pediatr* **181**, 1709-1718 (2022).

151. L. Yu *et al.*, Increased burden of de novo predicted deleterious variants in complex congenital diaphragmatic hernia. *Hum Mol Genet* **24**, 4764-4773 (2015).

152. E. Brosens *et al.*, Unraveling the Genetics of Congenital Diaphragmatic Hernia: An Ongoing Challenge. *Front Pediatr* **9**, 800915 (2021).

153. M. Bisserier *et al.*, Regulation of the Methylation and Expression Levels of the BMPR2 Gene by SIN3a as a Novel Therapeutic Mechanism in Pulmonary Arterial Hypertension. *Circulation* **144**, 52-73 (2021).

154. P. Feliciano *et al.*, Exome sequencing of 457 autism families recruited online provides evidence for autism risk genes. *NPJ Genom Med* **4**, 19 (2019).

155. M. X. Tang *et al.*, Incidence of AD in African-Americans, Caribbean Hispanics, and Caucasians in northern Manhattan. *Neurology* **56**, 49-56 (2001).

156. K. A. Engleka *et al.*, Insertion of Cre into the Pax3 locus creates a new allele of Splotch and identifies unexpected Pax3 derivatives. *Dev Biol* **280**, 396-406 (2005).

157. M. Logan *et al.*, Expression of Cre Recombinase in the developing mouse limb bud driven by a Prxl enhancer. *Genesis* **33**, 77-80 (2002).

158. W. Zhang *et al.*, Spatial-temporal targeting of lung-specific mesenchyme by a Tbx4 enhancer. *BMC Biol* **11**, 111 (2013).

159. K. Branchfield *et al.*, Pulmonary neuroendocrine cells function as airway sensors to control lung immune response. *Science* **351**, 707-710 (2016).

160. T. G. Hamilton, R. A. Klinghoffer, P. D. Corrin, P. Soriano, Evolutionary divergence of platelet-derived growth factor alpha receptor signaling mechanisms. *Mol Cell Biol* **23**, 4013-4025 (2003).

161. A. Dobin *et al.*, STAR: ultrafast universal RNA-seq aligner. *Bioinformatics* **29**, 15-21 (2013).

162. B. Li, C. N. Dewey, RSEM: accurate transcript quantification from RNA-Seq data with or without a reference genome. *BMC Bioinformatics* **12**, 323 (2011).

163. M. D. Robinson, D. J. McCarthy, G. K. Smyth, edgeR: a Bioconductor package for differential expression analysis of digital gene expression data. *Bioinformatics* **26**, 139-140 (2010).

164. Y. Hao *et al.*, Integrated analysis of multimodal single-cell data. *Cell* **184**, 3573-3587.e3529 (2021).

165. LungMAP. (LungMAP consortium and the LungMAP Data Coordinating Center (1U01HL122638)), vol. 2021.

ACKNOWLEDGEMENTS

We thank Gregory David (NYU Grossman School of Medicine) and Wei Shi (Keck School of Medicine, USC) for sharing mouse strains, the University of Wisconsin-Madison Gene Expression Center and Bioinformatics Resource Center for help conducting and analyzing the RNA-sequencing experiments, the University of Wisconsin Carbone Cancer Center FLOW Cytometry Laboratory where lung mesenchymal cell sorting was conducted, and the University of Wisconsin-Madison Optical Imaging Core and the University of California, San Diego School of Medicine Microscopy Core where the confocal imaging was conducted. We also thank Aki Ikeda and the members of the Ikeda laboratory (University of Wisconsin-Madison) and Xin Sun and members of the Sun laboratory (University of California, San Diego) for discussion and review of this manuscript.

We also thank the patients and family members who have participated in the DHREAMs (Diaphragmatic Hernia Research and Exploration; Advancing Molecular Science) study.

Funding:

Translational Science Career Development Award KL2TR000428 (DJM), a subaward from the National Center for Advancing Translational Sciences (NCATS) grant to the University of Wisconsin-Madison Institute for Clinical and Translational Research UL1TR000427

National Institutes of Health grants NHLBI R01HL146859 (DJM); NHLBI R01HL132366, R01HL136998, and X01HL140543 (YS and WKC); and NICHD P01HD068250 (YS, WKC, and DJM).

Author contributions

Conceptualization: WKC and DJM

Methodology: GS, NCC, JY, WKC, and DJM

Investigation: GS, ZL, NT, WG, MEB, MDW, GS, RH, JW, HT, DMT, AR, TAH, PZ, RM, and DJM

Funding Acquisition: YS, WKC, and DJM

Writing – original draft: GS and DJM

Writing – review & editing: GS, ZL, MEB, NCC, RM, YS, WKC, and DJM

Declaration of interests: Authors declare that they have no competing interests.

Figure 1.

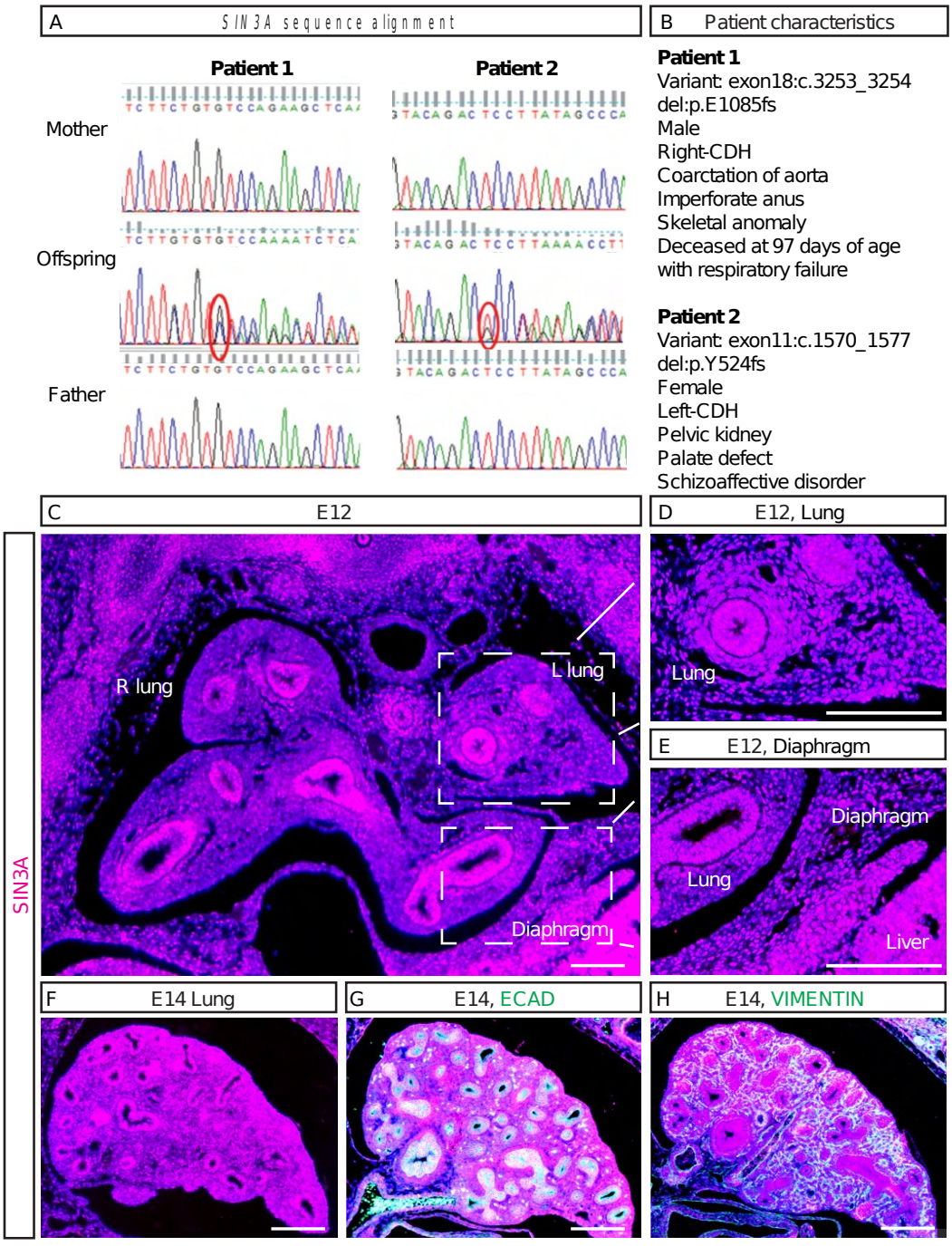

Figure 1. *SIN3A* sequence variants were present in patients with CDH and SIN3A is expressed in the developing lungs and diaphragm. (A, B) *De novo* sequence variants were identified in two patients with complex CDH. (C-E) *Sin3a* is broadly expressed in the developing lungs and

diaphragm of mice at embryonic day 12 (E12). (F-H) In the lungs, *Sin3a* is expressed at E14 (F) in both the *Cdh1*-expressing epithelium (E-cadherin, G) and *Vimentin*-expressing mesenchyme (H).

Figure 2.

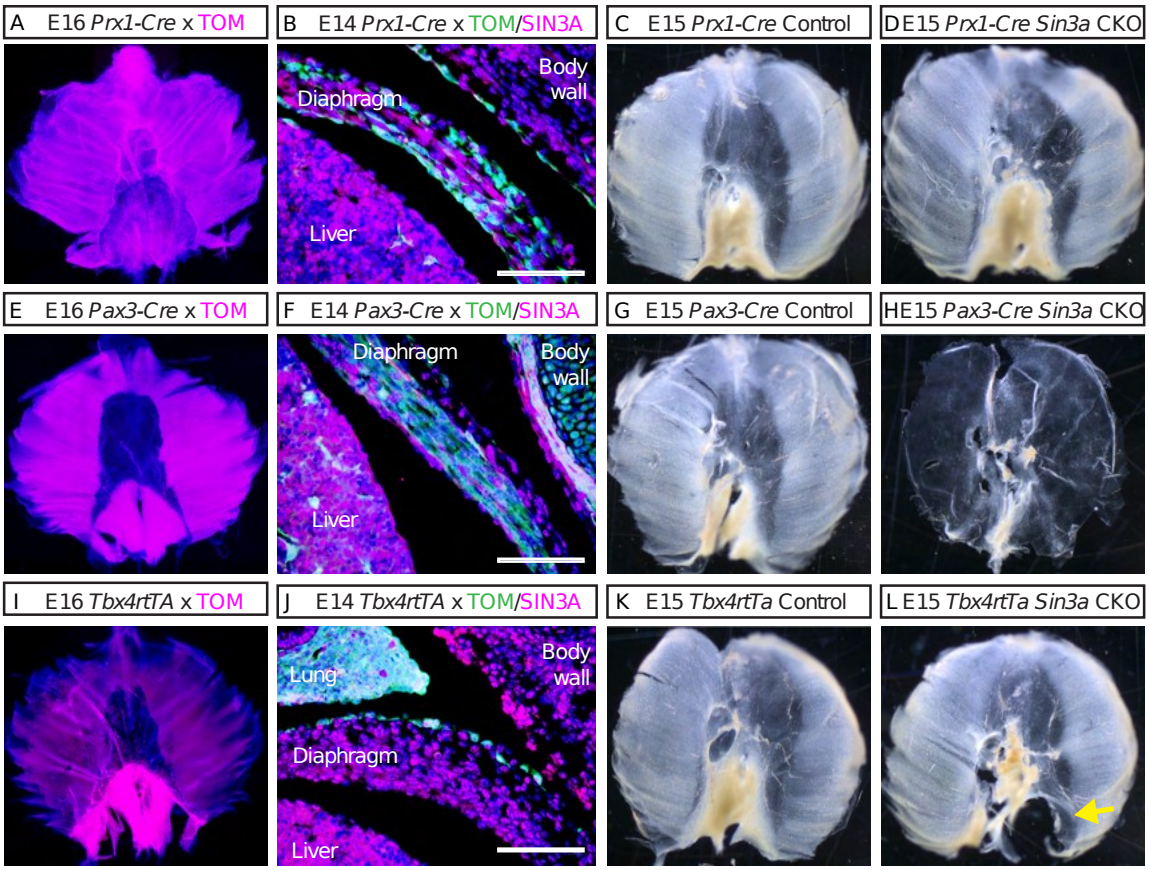

Figure 2. SIN3A is required for diaphragm development. (A, B) *Prx1-Cre* was used to induce recombination in diaphragm fibroblast cells that express *Sin3a*. (C, D) Compared to controls (C), *Prx1-Cre Sin3a* conditional deletion embryos (CKO) had normal diaphragm development at E15 (D). (E, F) *Pax3-Cre* was used to induce recombination in diaphragm skeletal muscle cells that express *Sin3a*. (G-H) Compared to controls (G), *Pax3-Cre Sin3a* CKO embryos had a thin, muscle-less diaphragm at E15 (H). (I, J) *Tbx4-rtTA; Tet-o-Cre* was used to induce recombination in the mesothelium that expresses *Sin3a*. (K, L) Compared to controls (K), *Tbx4-rtTA; Tet-o-Cre Sin3a* CKO embryos had a defect in the left posterior lateral portion of the diaphragm (L, yellow arrow) similar to the majority of patients with CDH.

Figure 3.

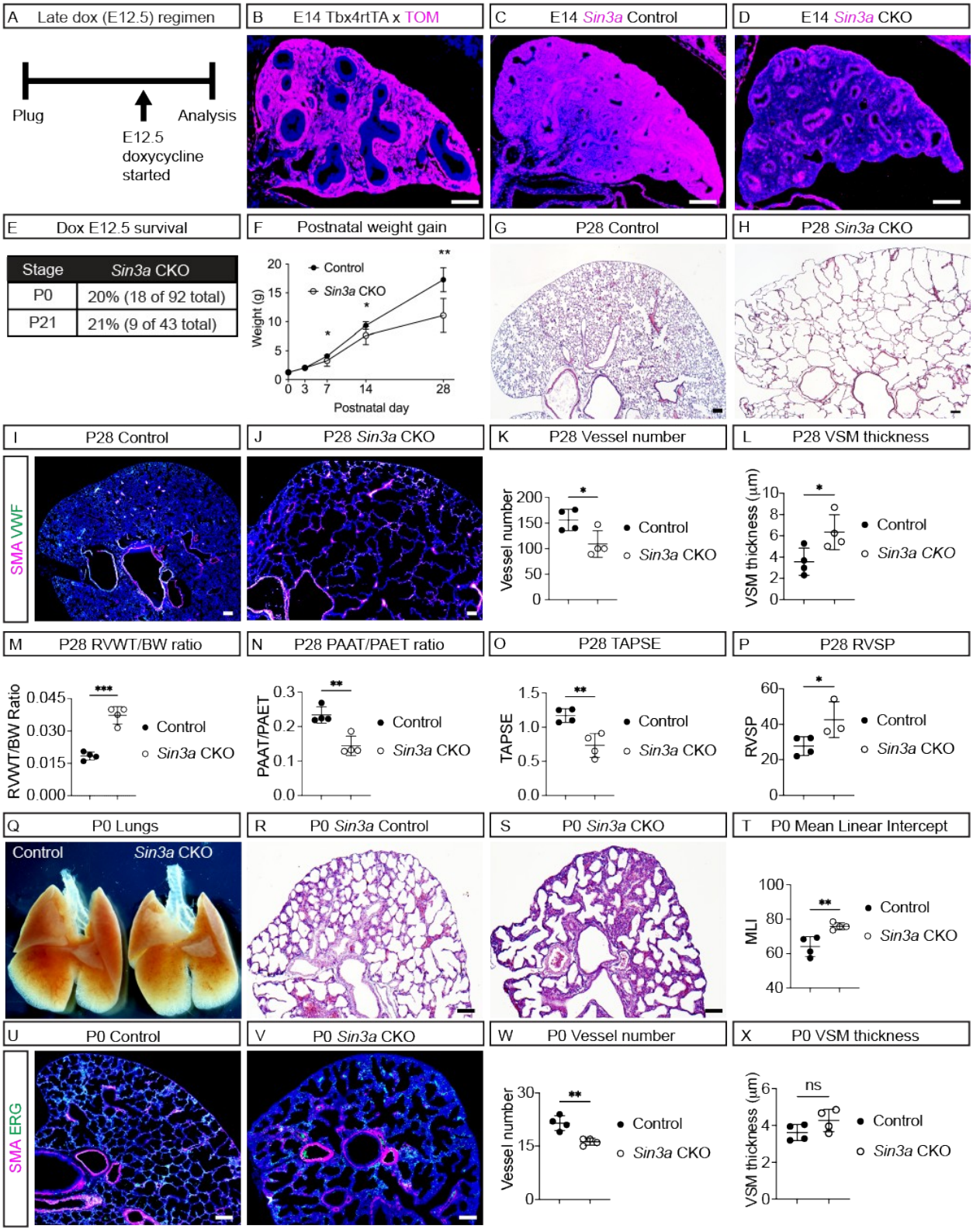
A Late dox (E12.5) regimen
Plug
Analysis
E12.5 doxycycline started
B E14 Tbx4rtTA x TOM
C E14 Sin3a Control
D E14 Sin3a CKO
E Dox E12.5 survival
Stage | Sin3a CKO
P0 | 20% (18 of 92 total)
P21 | 21% (9 of 43 total)
F Postnatal weight gain
Weight (g)
Control
Sin3a CKO
Postnatal day
G P28 Control
H P28 Sin3a CKO
I P28 Control
J P28 Sin3a CKO
SMA VWF
K P28 Vessel number
Vessel number
L P28 VSM thickness
VSM thickness (μm)
M P28 RVWT/BW ratio
RVWT/BW Ratio
N P28 PAAT/PAET ratio
PAAT/PAET
O P28 TAPSE
TAPSE
P P28 RVSP
RVSP
Q P0 Lungs
Control
Sin3a CKO
R P0 Sin3a Control
S P0 Sin3a CKO
T P0 Mean Linear Intercept
MLI
U P0 Control
V P0 Sin3a CKO
SMA ERG
W P0 Vessel number
X P0 VSM thickness
ns

Figure 3. SIN3A is required in the lung mesenchyme. (A, B) Late embryonic (E12) induction of *Tbx4-rtTA; Tet-o-Cre* with doxycycline (A) resulted in recombination throughout the lung mesenchyme (B). (C, D) E14 control lungs had broad expression of *Sin3a* (C) while *Tbx4-rtTA; Tet-o-Cre* CKO mice (*Sin3a* CKO) that underwent induction with doxycycline at E12.5 maintained expression of *Sin3a* in the epithelium but lacked *Sin3a* expression in the mesenchyme (D). (E-P) Despite surviving normally (E), *Sin3a* CKO mice did not gain weight as well as controls (F, P7 *p = 0.03, P14 *p = 0.04, P28 **p = 0.002). Compared to controls (G, I), *Sin3a* CKO mice had emphysematous and simplified distal airspaces (H), abnormal pulmonary vasculature (J) with decreased lung vessel number (K, *p = 0.03) and smooth muscle hypertrophy (L, *p = 0.04), and pulmonary hypertension with right ventricular hypertrophy (M, RVWT/BW ***p = 0.0008), increased pulmonary vascular resistance (N, PAAT/PAET ratio **p = 0.003), decreased right ventricular function (O, TAPSE **p = 0.008), and increased peak systolic right ventricular pressure (P, RVSP *p = 0.04). (Q-X) Lung defects were first evident in *Sin3a* CKO mice at P0. Despite having normal gross lung morphology (Q), *Sin3a* CKO mice had thickened lung interstitium and simplification of airspaces measured by MLI (R-T, MLI **p = 0.008) and decreased lung vessel number (U-W, **p = 0.004) with no smooth muscle hypertrophy (X, ns p = 0.13). Dox: doxycycline, TOM: tomato, SMA: smooth muscle alpha actin, VWF: von Willebrand factor, RVWT/BW: right ventricle wall thickness to body weight ratio, PAAT/PAET: pulmonary artery acceleration time to pulmonary artery ejection time ratio, TAPSE: tricuspid valve annular plane excursion during systole, RVSP: right ventricle peak systolic pressure, MLI: mean linear intercept, ERG: Ets related gene.

Figure 4.

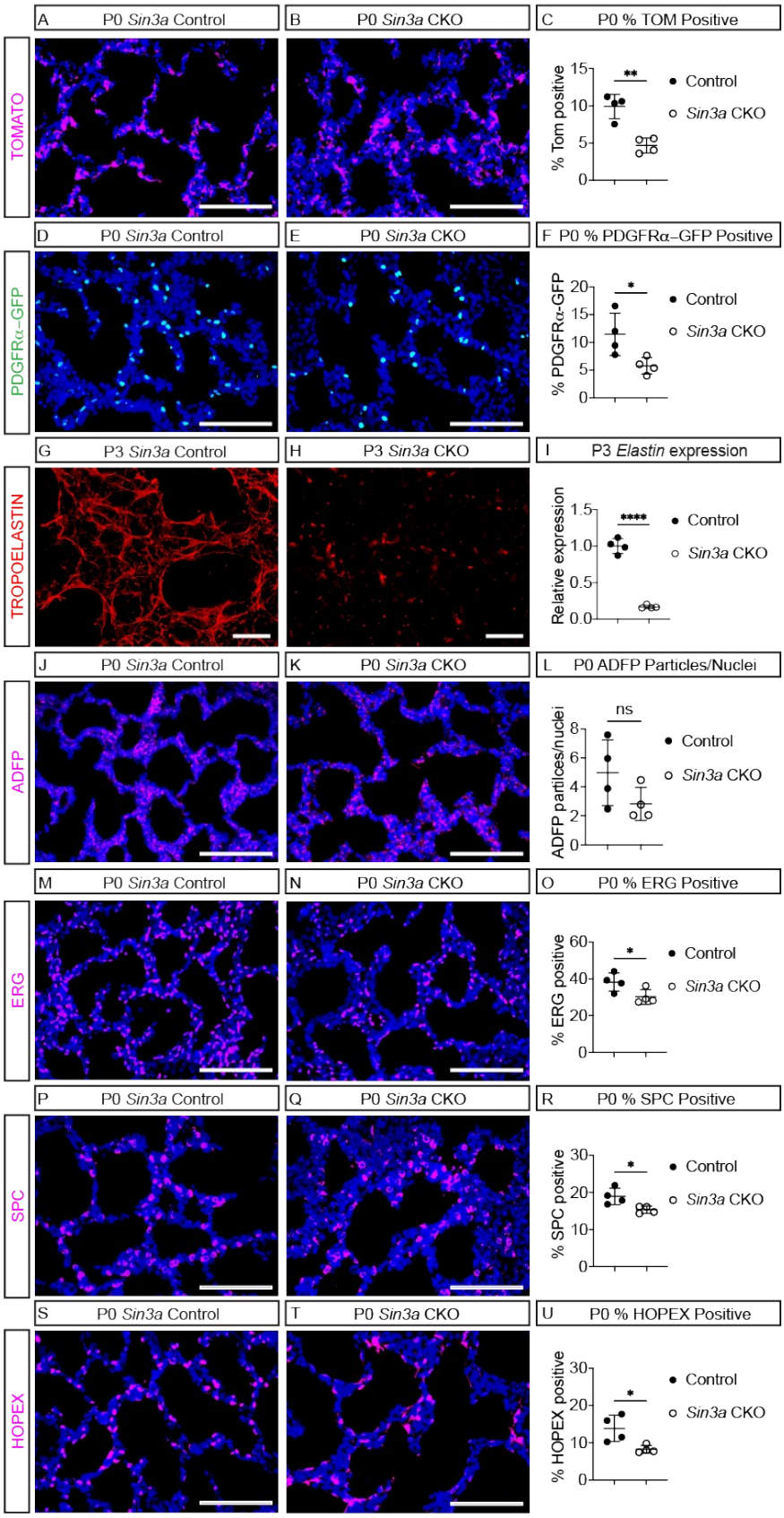
A P0 Sin3a Control
B P0 Sin3a CKO
C P0 % TOM Positive
TOMATO
% Tom positive
Control
Sin3a CKO
D P0 Sin3a Control
E P0 Sin3a CKO
F P0 % PDGFRα–GFP Positive
PDGFRα–GFP
% PDGFRα-GFP
G P3 Sin3a Control
H P3 Sin3a CKO
I P3 Elastin expression
TROPOELASTIN
Relative expression
J P0 Sin3a Control
K P0 Sin3a CKO
L P0 ADFP Particles/Nuclei
ADFP
ADFP particles/nuclei
ns
M P0 Sin3a Control
N P0 Sin3a CKO
O P0 % ERG Positive
ERG
% ERG positive
P P0 Sin3a Control
Q P0 Sin3a CKO
R P0 % SPC Positive
SPC
% SPC positive
S P0 Sin3a Control
T P0 Sin3a CKO
U P0 % HOPEX Positive
HOPEX
% HOPEX positive

Figure 4. SIN3A is required in the lung mesenchyme for mesenchymal cell, extracellular matrix, endothelial cell, and alveolar epithelial cell development. (A-I) Compared to controls (A, D, G), P0 *Sin3a* CKO mice had a lower percentage of lung mesenchymal cells that underwent recombination (B, C, ** p = 0.003) and *Pdgfra*-GFP positive myofibroblast precursor cells (E, F, * p = 0.03) with decreased extracellular matrix (H) and decreased *Elastin* expression (I, **** p < 0.0001) at P3. Despite the loss of SIN3A, compared to controls (J), P0 *Sin3a* CKO mice maintained *Plin2* expressing lipofibroblast precursor cells quantified as the ratio of ADFP-labelled particles to DAPI-stained nuclei (K, L, p = 0.1). (M-U) Compared to controls (M, P, and S) P0 *Sin3a* CKO mice had a lower percentage of endothelial cells labelled by ERG (N, O, * p = 0.04), type II alveolar epithelial cells labelled by SPC (Q, R, * p = 0.04), and type I alveolar epithelial cells labelled by HOPEX (T, U, * p = 0.04).

Figure 5.

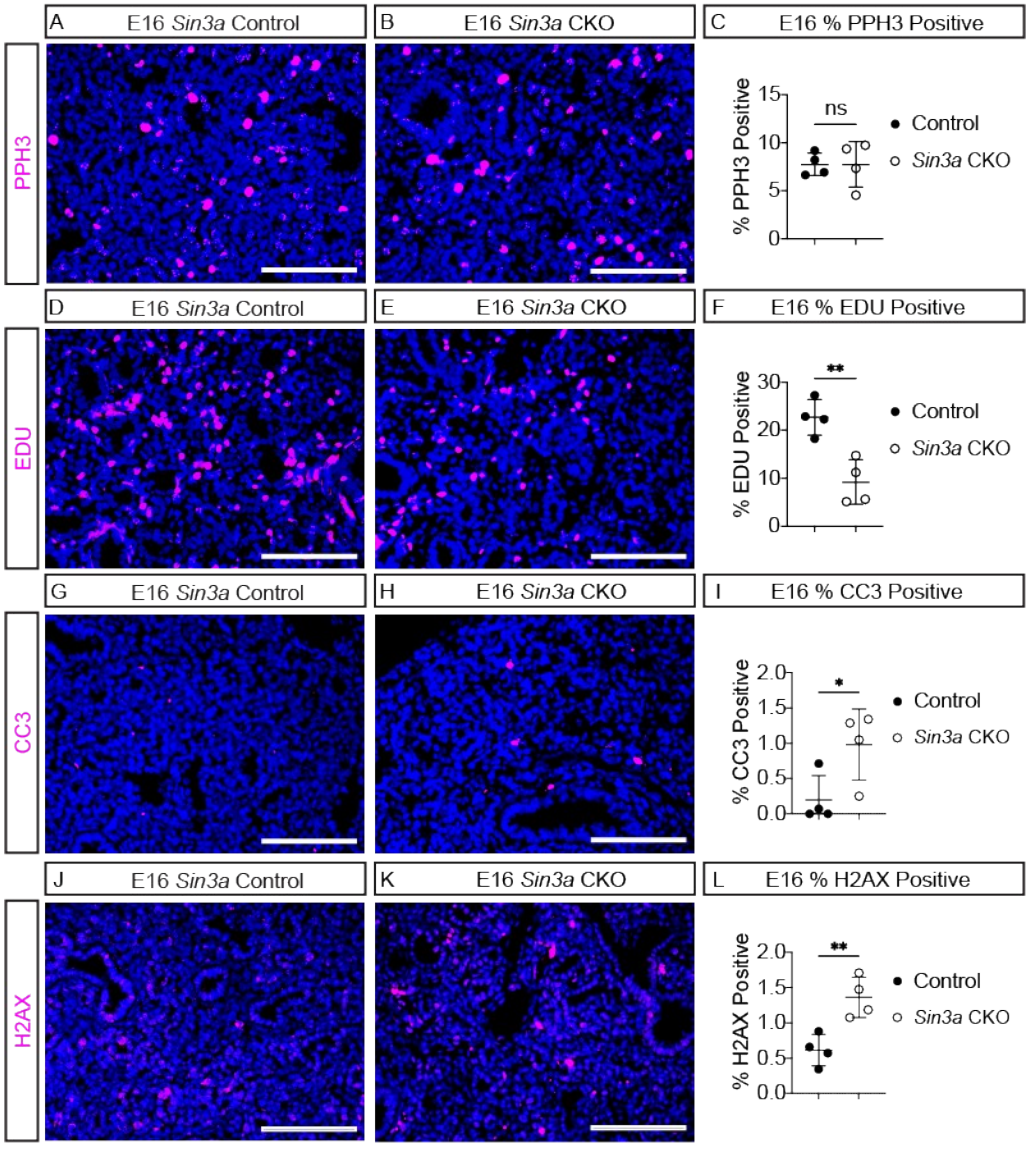

Figure 5. SIN3A is required for regulation of cell cycling, apoptosis, and DNA damage. (A-F) In contrast to controls at E16 (A, D), *Sin3a* CKO lungs had normal cell proliferation indicated by PPH3 staining (B, C, p = 0.99) but reduced G1 to S-phase transition indicated by EDU staining (E, F, ** p = 0.004). (G-I) Loss of SIN3A was associated with increased apoptosis indicated by CC3 staining in *Sin3a* CKO lungs (H, I, * p = 0.04) compared to controls (G). (J-L) Compared to

controls (J), *Sin3a* CKO lungs had increased H2AX staining indicating increased DNA damage (K, L, ** p = 0.007).

Figure 6.

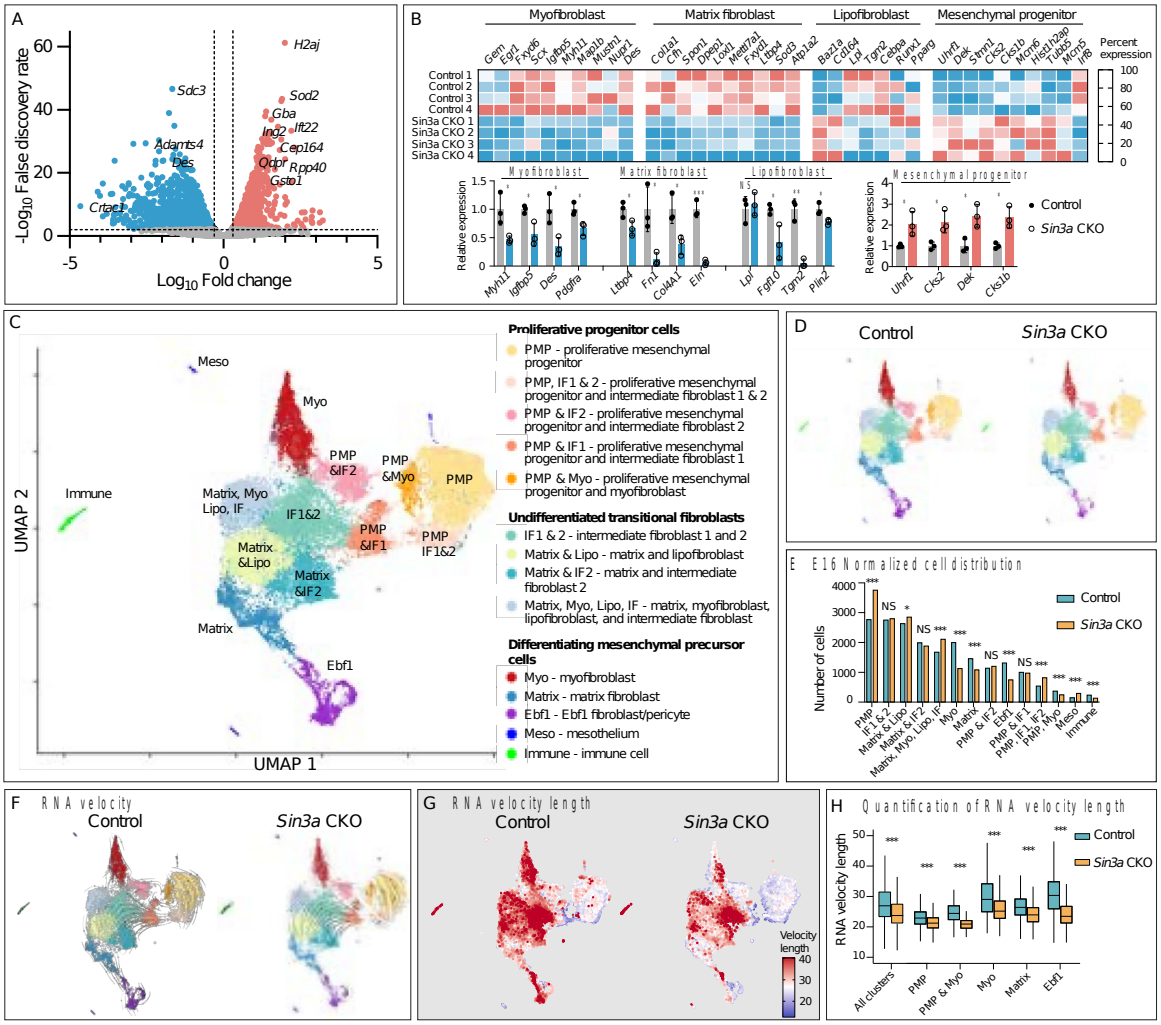

Figure 6. SIN3A directs mesenchymal cell differentiation. (A-B) Gene expression analysis conducted using RNA extracted from recombined lung mesenchymal cells of *Sin3a* CKO embryos showed that more than 4000 genes were mis-regulated in this cell population compared to controls (A, genes with – $\log_{10}$ false discovery rate > 2 and $\log_{10}$ fold change > 0.301 or < -0.301 (dotted lines) with increased expression are colored red or decreased expression are colored blue). Among the 100 most significantly mis-regulated genes were those identified in the bulk lung gene expression analysis (*Gba*, *Ift22*, *Qdpr*, and *Rpp40,* Supplemental Figure 5), expressed in myofibroblasts (*Des*) or extracellular matrix (*Gsto1* and *AdamTs4*), that regulate

apoptosis (*Sod2*, *Ing2*) and that encode SIN3 associated proteins (SAPS: *Ing2*, A). Compared to controls, the normalized percent expression of myofibroblast, matrix fibroblast, and lipofibroblast genes was decreased in *Sin3a* CKO lung mesenchymal cells while the expression of proliferating lung mesenchymal cell progenitor genes was increased (B). qRT-PCR analysis of gene expression using whole lung RNA extracts at E16 confirmed that genes expressed in myofibroblasts (*Myh11* * p = 0.03, *Igfbp5* * p 0.02, *Des* * p = 0.02, and *Pdgfrα* * p = 0.02), matrix fibroblasts (*Ltbp4* * p = 0.04, *Fn1* * p = 0.02, *Col4a1* * p = 0.02, *Eln* *** p = 0.0005), and lipofibroblasts (*Lpl* p = 0.63, *Fgf10* * p = 0.03, *Tgm2* ** p = 0.001, *Adfp* * p = 0.03) were decreased in expression while genes expressed in proliferating mesenchymal progenitor cells (*Uhrf1* * p = 0.03, *Cks2* * p = 0.02, *Dek* * p = 0.01, *Cks1b* * p = 0.01) were increased in *Sin3a* CKO lungs (B). (C-H) Single cell RNA-sequencing of sorted recombined lung mesenchymal cells at E16 demonstrated that these cells included 3 groups: proliferative mesenchymal progenitor cells (PMPs), undifferentiated transitional fibroblasts, and differentiating mesenchymal precursor cells (C). (D-E) Mesenchymal cells collected from *Sin3a* CKO mice demonstrated a shift in population distribution with an increase in PMPs and decrease in differentiating mesenchymal precursor cells (D-E) with the most significant decrease observed in myofibroblasts (E, PMP *** p = $2.67x10^{-26}$; IF1 &2 NS p = 0.59; Matrix and Lipo * p = 0.02; Matrix and IF2 NS p = 0.15; Matrix, Myo, Lipo, IF *** p = $6.36x10^{-9}$; Myo *** p = $7.63x10^{-39}$; Matrix *** p = $7.43X10^{-10}$; PMP & IF2 NS p = 0.20; Ebf1 *** p = $7.86x10^{-26}$; PMP and IF1 NS p = 0.58; PMP, IF1, IF2 *** p = $2.18X10^{-10}$; PMP, Myo *** p = $6.66x10^{-5}$; Meso *** p = 3.67 x 10^{-9}; Immune *** p = $4.92x10^{-6}$). (F-H) RNA velocity analysis demonstrated the differentiation potential of recombined mesenchymal cells in *Sin3a* CKO and control cells (F). (G, H) Comparison of the RNA velocity lengths demonstrated that loss of SIN3A was associated with

decreased RNA velocity length in all clusters (H, *** $p = 4.72x10^{-281}$) as well as in proliferative mesenchymal progenitor cells (H, PMP *** $p = 8.02x10^{-20}$ and PMP/myofibroblast *** $p = 2.20x10^{-9}$) and differentiating mesenchymal precursor cells (H, myofibroblast *** $p = 2.30x10^{-32}$, matrix fibroblast *** $p = 2.09x10^{-15}$, and Ebf1 fibroblast cells *** $p = 3.51x10^{-46}$).

Figure 7.

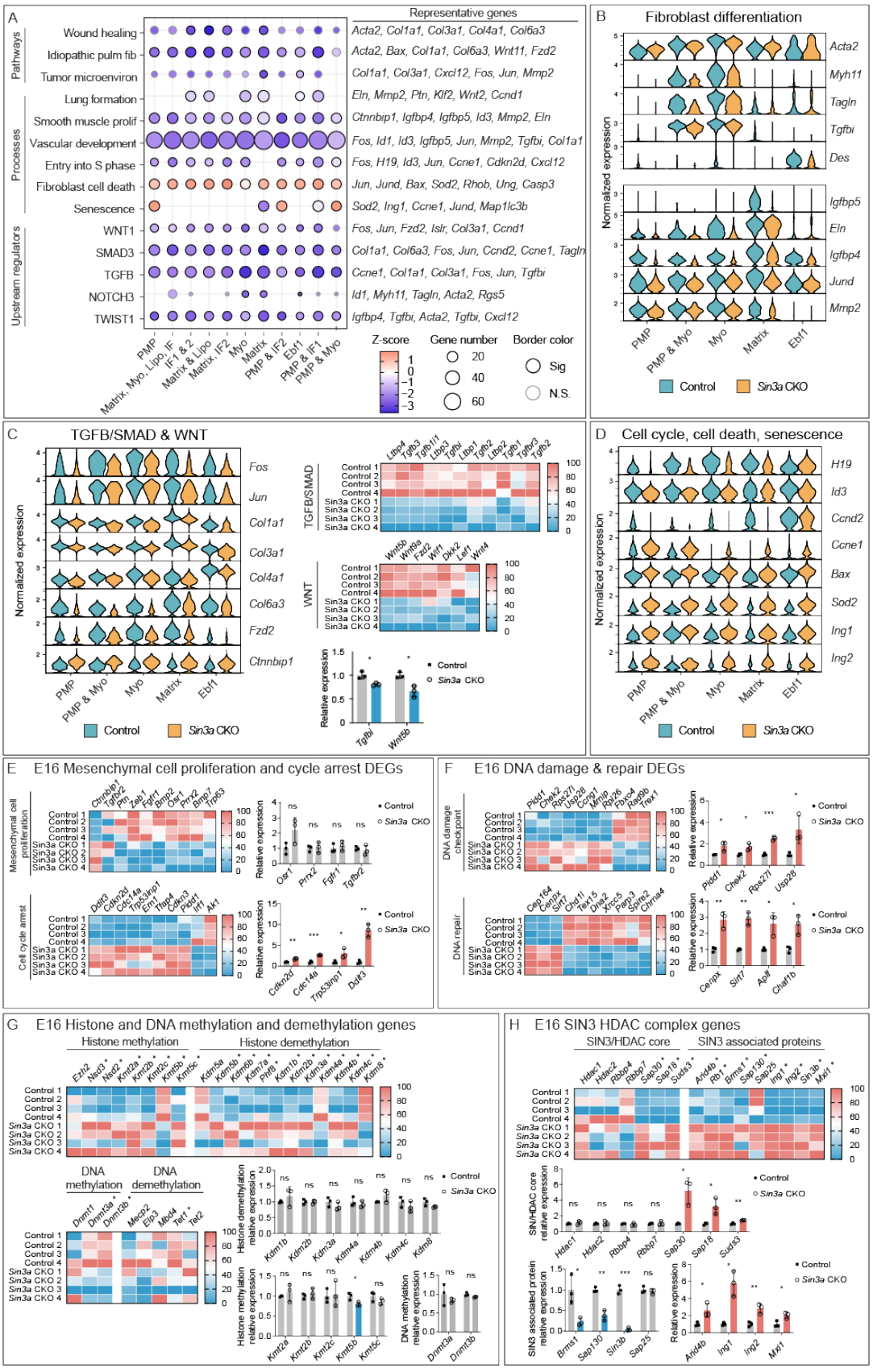
A
Pathways
Processes
Upstream regulators
Wound healing
Idiopathic pulm fib
Tumor microenviron
Lung formation
Smooth muscle prolif
Vascular development
Entry into S phase
Fibroblast cell death
Senescence
WNT1
SMAD3
TGFB
NOTCH3
TWIST1
Representative genes
Acta2, Col1a1, Col3a1, Col4a1, Col6a3
Acta2, Bax, Col1a1, Col6a3, Wnt11, Fzd2
Col1a1, Col3a1, Cxcl12, Fos, Jun, Mmp2
Eln, Mmp2, Ptn, Klf2, Wnt2, Ccnd1
Ctnnbip1, Igfbp4, Igfbp5, Id3, Mmp2, Eln
Fos, Id1, Id3, Igfbp5, Jun, Mmp2, Tgfbi, Col1a1
Fos, H19, Id3, Jun, Ccne1, Cdkn2d, Cxcl12
Jun, Jund, Bax, Sod2, Rhob, Ung, Casp3
Sod2, Ing1, Ccne1, Jund, Map1lc3b
Fos, Jun, Fzd2, Islr, Col3a1, Ccnd1
Col1a1, Col6a3, Fos, Jun, Ccnd2, Ccne1, Tagln
Ccne1, Col1a1, Col3a1, Fos, Jun, Tgfbi
Id1, Myh11, Tagln, Acta2, Rgs5
Igfbp4, Tgfbi, Acta2, Tgfbi, Cxcl12
PMP
Matrix, Myo, Lipo, IF
IF1 & 2
Matrix & Lipo
Matrix, IF2
Myo
Matrix
PMP & IF2
Ebf1
PMP & IF1
PMP & Myo
Z-score
1
0
−1
−2
−3
Gene number
20
40
60
Border color
Sig
N.S.
B
Fibroblast differentiation
Normalized expression
Acta2
Myh11
Tagln
Tgfbi
Des
Igfbp5
Eln
Igfbp4
Jund
Mmp2
PMP
PMP & Myo
Myo
Matrix
Ebf1
Control
Sin3a CKO
C
TGFB/SMAD & WNT
Normalized expression
Fos
Jun
Col1a1
Col3a1
Col4a1
Col6a3
Fzd2
Ctnnbip1
PMP
PMP & Myo
Myo
Matrix
Ebf1
Control
Sin3a CKO
TGFB/SMAD
Ltbp4 Tgfb3 Tgfb1i1 Ltbp3 Tgfbi Ltbp1 Tgfb2 Ltbp2 Tgfb1 Tgfbr3 Tgfb2
WNT
Wnt5b Wnt9a Fzd2 Wif1 Dkk2 Lef1 Wnt4
Control 1
Control 2
Control 3
Control 4
Sin3a CKO 1
Sin3a CKO 2
Sin3a CKO 3
Sin3a CKO 4
Relative expression
Tgfbi
Wnt5b
Control
Sin3a CKO
D
Cell cycle, cell death, senescence
Normalized expression
H19
Id3
Ccnd2
Ccne1
Bax
Sod2
Ing1
Ing2
PMP
PMP & Myo
Myo
Matrix
Ebf1
Control
Sin3a CKO
E
E16 Mesenchymal cell proliferation and cycle arrest DEGs
Mesenchymal cell proliferation
Ctnnbip1 Tgfbr2 Ptn Zeb1 Fgfr1 Bmp2 Osr1 Prrx2 Bmp7 Trp63
Cell cycle arrest
Ddit3 Cdkn2d Cdc14a Trp53inp1 Ern1 Thbs4 Cdkn1a Pkdrl Irf1 Ak1
Relative expression
Osr1
Prrx2
Fgfr1
Tgfbr2
Cdkn2d
Cdc14a
Trp53inp1
Ddit3
Control
Sin3a CKO
F
E16 DNA damage & repair DEGs
DNA damage checkpoint
Pkd1l Chek2 Rps27l Usp28 Ccng1 Mmp Rpr26 Fbxo4 Rad9b Trex1
DNA repair
Cep164 Cenpx Sirt1 Chd1l Tex15 Dnaj2 Xrcc5 Pam3 Sfmr2 Chrne4
Relative expression
Pkd1l
Chek2
Rps27l
Usp28
Cenpx
Sirt1
Apif
Chaf1b
Control
Sin3a CKO
G
E16 Histone and DNA methylation and demethylation genes
Histone methylation
Histone demethylation
Ezh2 Nsd3 Nsd2 Kmt2a Kmt2b Kmt2c Kmt5b Kmt5c
Kdm5a Kdm5b Kdm6b Kdm7a Phf8 Kdm1b Kdm2b Kdm3a Kdm4a Kdm4b Kdm4c Kdm8
DNA methylation
DNA demethylation
Dnmt1 Dnmt3a Dnmt3b Mecp2 Elp3 Mbd4 Tet1 Tet2
Histone demethylation relative expression
Kdm1b Kdm2b Kdm3a Kdm4a Kdm4b Kdm4c Kdm8
Histone methylation relative expression
Kmt2a Kmt2b Kmt2c Kmt5b Kmt5c
DNA methylation relative expression
Dnmt3a Dnmt3b
Control
Sin3a CKO
H
E16 SIN3 HDAC complex genes
SIN3/HDAC core
SIN3 associated proteins
Hdac1 Hdac2 Rbbp4 Rbbp7 Sap30 Sap18 Suds3
Arid4b Rbl1 Brms1 Sap130 Sap25 Ing1 Ing2 Sin3b Mxi1
SIN/HDAC core relative expression
Hdac1
Hdac2
Rbbp4
Rbbp7
Sap30
Sap18
Suds3
SIN3 associated protein relative expression
Brms1
Sap130
Sin3b
Sap25
Relative expression
Arid4b
Ing1
Ing2
Mxi1
Control
Sin3a CKO

Figure 7. SIN3A is required for regulation of mesenchymal cell differentiation, cell cycling, DNA damage, and senescence. (A-D) Integrated pathway analysis (IPA) of differential gene expression demonstrated that loss of SIN3A resulted in altered gene expression in pathways important for lung development and mesenchymal cell differentiation (A). (A, B) Pathway analysis demonstrated that the expression of genes required for mesenchymal cell differentiation, specifically myofibroblast and matrix fibroblast differentiation, was decreased by loss of SIN3A (B). (C) Both TGFB and WNT pathways were downregulated in *Sin3a* CKO mesenchymal cells. These data were confirmed by the percent expression of TGFB and WNT genes in bulk recombined mesenchymal RNA-sequencing and in the relative expression of *Tgbi* and *Wnt5b* in qRT-PCR analysis of whole lung RNA extracts (C). (D) IPA analysis demonstrated decreased expression of genes that promote cell cycling (*H19*, *Id3*, and *Ccnd2*) with increased expression of genes that promote cell death and senescence (*Ccne1*, *Bax*, *Sod2*, *Ing1*) in *Sin3a* CKO recombined mesenchymal cells. (E-F) Loss of SIN3A resulted in altered expression of genes that regulate mesenchymal cell proliferation (E) and in genes expressed in response to DNA damage or that regulate DNA repair (F). (E) Normalized percent expression of genes that promote mesenchymal cell proliferation was decreased while expression of genes that promote cell cycle arrest was increased in recombined *Sin3a* CKO lung mesenchymal cells. Whole lung gene expression analysis at E16 showed no change in genes that promote mesenchymal cell proliferation (*Osr1* p = 0.08, *Prrx2* p = 0.78, *Fgfr1* p =0.52, *Tgfbr2* p = 0.58) whereas expression of genes that promote cell cycle arrest was increased (*Cdkn2d* **p = 0.002, *Cdc14a* *** p = 0.0007, *Trp53inp1* * p = 0.04, *Ddit* ** p = 0.001) in *Sin3a* CKO lungs (E). (F) Genes expressed in response to DNA damage or associated with DNA repair were mis-regulated in *Sin3a* CKO

lung mesenchymal cells. Whole lung gene expression analysis demonstrated that genes expressed in response to DNA damage (*Pidd1* * p = 0.03, *Chek2* * p = 0.03, *Rps27I* *** p = 0.0003, *Usp28* * p 0.04) or associated with DNA repair (*Cenpx* ** p = 0.004, *Sirt7* ** p = 0.001, *Aplf* * p = 0.02, *Char1b* * p = 0.01) were increased in *Sin3a* CKO lungs (F). (G) Normalized percent expression of genes associated with histone methylation (*Nsd3*, *Nsd2*, *Kmt2a*, *Kmt2b*, *Kmt2c*, *Kmt5b*, and *Kmt5c*) and demethylation (*Kdm5b*, *Kdm6b*, *Kdm7a*, *Phf8*, *Kdm1b*, *Kdm2b*, *Kdm3a*, *Kdm4a*, *Kdm4b*, *Kdm4c*, *Kdm8*) and DNA methylation (*Dnmt3a*, *Dnmt3b*) and demethylation (*Tet1*) was abnormal in *Sin3a* CKO lung mesenchymal cells at E16. Whole lung gene expression at E16 demonstrated that only histone demethylase *Kmt5b* was decreased in expression (*p = 0.03) in *Sin3a* CKO lungs. (H) Normalized percent expression of genes that encode SIN3/HDAC core complex proteins (*Sap30*, *Sap18*, and *Suds3*) and SIN3 associated proteins (SAPs: *Arid4b*, *Rb1*, *Brms1*, *Sap130*, *Ing1*, *Ing2*, *Sin3b*, and *Mxi1*) was increased in *Sin3a* CKO lung mesenchymal cells at E16. Whole lung gene expression at E16 showed that SIN3/HDAC core complex genes *Sap30* (*p = 0.01), *Sap18* (*p = 0.02), and *Suds3* (** p = 0.004) were increased in expression. SAP encoding genes *Brms1* (*p = 0.02) and *Sap130* (** p = 0.001) were decreased in expression while *Arid4b* (*p = 0.03), *Ing1* (**p 0.005), *Ing2* (**p = 0.007), and *Mxi1* (*p = 0.02) were increased in *Sin3a* CKO lungs (H).

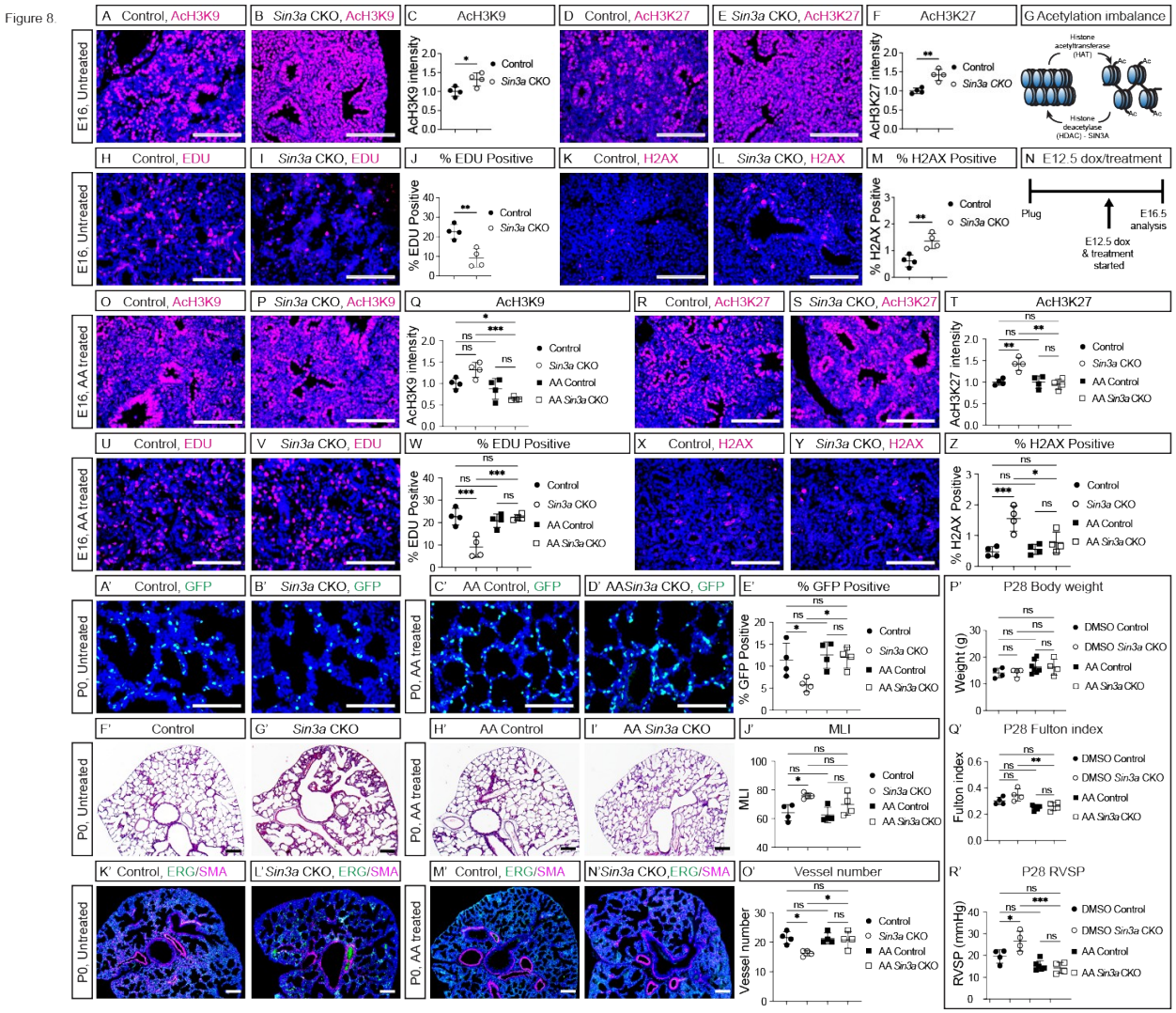

Figure 8. Embryonic inhibition of histone acetyltransferase (HAT) rescued lung mesenchyme and pulmonary vascular defects in *Sin3a* CKO mice. (A-G) Compared to controls at E16, *Sin3a* CKO mice had increased acetylated H3K9 (B, C, *p = 0.03) and H3K27 (E, F, **p = 0.002) suggesting an imbalance of histone acetylation/deacetylation in mice lacking SIN3A (G). (H-Z) E16 *Sin3a* CKO embryos (I, L) had decreased G1 to S-phase transition (J, **p = 0.004) and increased DNA damage (M, **p = 0.007) indicated by H2AX staining compared to controls (H, K). Embryonic treatment with anacardic acid (AA), was started at E12 when doxycycline

induced deletion of *Sin3a* was initiated (N). Compared to untreated *Sin3a* CKO mice (A-M), AA treated *Sin3a* CKO mice (N) had decreased acetylated H3K9 (P, Q, ***p = 0.0004) and H3K27 (S, T, **p = 0.001) that was less than or similar to untreated control (A, Q, *p = 0.04, D, T, p =0.94) and AA treated controls (O, Q, p = 0.25, R, T, p = 0.94). AA treated *Sin3a* CKO mice had increased G1 to S-phase transition (V) compared to untreated *Sin3a* CKOs (I, W, ***p = 0.0007) that was similar to untreated controls (H, W, p = 0.99) and controls treated with AA (U, W, p = 0.92). DNA damage was decreased in *Sin3a* CKO mice treated with AA (Y) compared to untreated *Sin3a* CKO mice (L, Z, *p = 0.01) but was similar to untreated control mice (D, Z, p = 0.98) and controls treated with AA (X, Z, p = 0.70). P0 *Sin3a* CKO mice treated with AA had increased *Pdgfrα*-GFP labelled myofibroblast precursor cells (D') compared to untreated *Sin3a* CKO mice (B', E', *p = 0.04). P0 *Sin3a* CKO mice treated with AA had a similar number of *Pdgfrα*-GFP labelled myofibroblast precursor cells (D') compared to untreated controls (A', E' p = 0.94) and controls treated with AA (C', E', p = 0.99). Embryonic treatment with AA did not change distal airspace morphology in controls treated with AA (H') compared to untreated controls (F', J', p = 0.98). Embryonic treatment with AA did not significantly change airspace simplification in *Sin3a* CKO lungs (I') compared to untreated *Sin3a* CKO lungs (G', J', p = 0.47); however, the MLI of AA treated *Sin3a* CKO lungs (I', J') was similar to untreated controls (F', J', p = 0.47) and AA treated controls (H', J', p = 0.29). The number of pulmonary vessels in AA treated *Sin3a* CKO mice at P0 (N') was increased compared to untreated *Sin3a* CKO mice (L', O' *p = 0.04) and was similar to untreated controls (K', O', p = 0.95) and AA treated controls (M', O', p = 0.99). AA treated control and *Sin3a* CKO mice gained weight after birth and were a similar size to DMSO vehicle treated controls at P28 (P'). Compared to DMSO treated *Sin3a* CKO mice, AA treated *Sin3a* CKO mice had a lower Fulton index (Q', **p =

0.003) that was similar to DMSO treated controls (Q', p = 0.21) and AA treated controls (Q', p = 0.97). The peak systolic pressure in the right ventricle was lower in AA treated *Sin3a* CKO mice compared to DMSO treated *Sin3a* CKO mice (R', ***p = 0.0004) and was similar to DMSO treated controls (R', p = 0.13) and AA treated controls (R', p = 0.96).